Adaptation of existing cardiovascular simulation model to cardiac pumping physiology

EMMA TÖRNER

2017

LUND UNIVERSITY

MASTER'S THESIS
IN BIOMEDICAL ENGINEERING

DEPARTMENT OF BIOMEDICAL ENGINEERING

SUPERVISORS: FELICIA SEEMANN & EINAR HEIBERG

Abstract

Cardiovascular diseases, affecting the heart and blood vessels, are the most common cause of death globally. However, the risk of suffering from a cardiovascular disease could decrease significantly as research improve treatment and identification of symptoms. One way to increase our knowledge and improve education of the cardiovascular system is to develop mathematical simulation models. This thesis project will attend the subject of cardiovascular modeling by analyzing an already implemented simulation model, the CircAdapt model. The project aim to thoroughly analyze the model from a physiological perspective and to derive the mathematical equations constituting the model. In addition to the analysis, extensions to the model have been developed, with the purpose of improving the model structure of the heart to anatomy and known qualities of cardiac pumping. Conclusions of the thesis are that the CircAdapt model well describes the dynamics of the cardiovascular system and consider both physical and physiological properties in its construction. Model limitations in the aspect of cardiovascular physiology have been identified. However, the highest physiological accuracy is the second priority after numerical stability, which can be hard to achieve when working with biomedical modeling. Several adaptations have been executed to improve heart anatomy and physiology. The adaptations differ in accuracy and are in need of future work to improve model stability.

Keywords: The CircAdapt model, biomedical modeling, cardiovascular, cardiac pumping, simulation.

Contents

Populärvetenskaplig sammanfattning

Hjärtat pumpar blod ut i kroppen mellan 40 och 100 gånger per minut. Drygt en tredjedel av alla dödsfall orsakas av hjärt- och kärlsjukdomar och ett sjukt hjärta kan därmed leda till fatala konsekvenser. Hjärt- och kärlsjukdomar är följaktligen den vanligaste dödsorsaken globalt och i Sverige.

Kroppens cirkulationssystem, som består av hjärta och blodkärl, är ett komplext system där vår kunskap och förståelse för dess funktion är livsviktigt för att identifiera och behandla hjärt- och kärlsjukdomar. Ett sätt att analysera och öka våra kunskaper om hjärtat och blodcirkulationen är att utveckla matematiska modeller.

En matematisk modell är att sätt att utnyttja matematik och fysikaliska principer för att beskriva hur ett system fungerar. Modellen konstrueras utefter kända kunskaper om det verkliga systemet och bidrar sedan med en, av systemet, förenklad bild. Idag finns flera matematiska modeller över människans cirkulationssystem som används i syfte att bidra till utbildning och forskning. Under examensarbetet har fokus legat på CircAdaptmodellen, som är en matematisk modell över cirkulationssystemet.

Att betrakta cirkulationssystemet matematiskt leder ofta till en prioritering av modellens funktion framför dess noggrannhet och korrekthet. Att en modell når en fysiologiskt rimlig lösning betecknas som en stabil modell, vilket ofta är svårt att åstadkomma när man modellerar fysiologiska system. Trots detta kan matematiska modeller komma att bli en tillgång inom forskning och behandling av hjärt- och kärlsjukdomar. Direkt ställs då kravet på bättre och mer korrekta modeller.

Det är numera känt från magnetresonanstomografi att hjärtats pumpning kan delas in i två komponenter. En kramande pumpning och en pumpning av blod längs med hjärtat likt en cykelpump. Den cykelpumpsliknande pumpningen av blod i hjärtat är viktig för hjärtats effektivitet och funktion och kan indikera risker för hjärtproblem. Trots detta är hjärtats pumpning något som ofta förenklas för mycket i matematiska modeller. Examensarbetet har därför utförts i syfte att analysera CircAdaptmodellen för att förstå dess funktion och uppbyggnad. Därefter har modellen adapterats för att på ett mer korrekt sätt modellera hjärtats uppbyggnad och dess pumpning.

CircAdaptmodellen som analyserats under examensarbetet är bra nog att bidra till kunskap och förståelse kring hjärtats uppbyggnad och funktion. Att utveckla modellens matematiska beskrivning av hjärtats pumpning är följaktligen viktigt för att utvidga modellens användningsområde. Examensarbetet har tagit ett första steg i den här utvecklingen genom att förbättra modellens beskrivning av hjärtats anatomi och pumpfunktion. Flera förändringar har gjort med varierad framgång och vidare arbete behövs. Slutsatsen är att det är svårare än man tror att nå en både korrekt och stabil modell när man modellerar hjärtat matematiskt.

Emma Törner
Lunds Tekniska Högskola

Acknowledgements

I wish to express my gratitude to the **Cardiac MR-group** at the Department of Clinical Physiology at Skåne University Hospital, for welcoming me as a part of the group during my thesis project. **Per** and **David**, for teaching me physiology and for always providing long discussions to questions I believed had a short and simple answer. **Sebastian**, for showing an interest in my thesis and making me reflect on my work. I also wish to send my appreciation to **Theo Arts**, **Joost Lumens** and the rest of the **CircAdapt Research Team**, for developing a model resulting in a challenging and interesting thesis project and for taking the time to answer my questions. To my **family** and **friends** for listening and supporting me during success and failure. Thank you **Einar**, my co-supervisor, for your great knowledge, ideas and discussions along the way. My sincerest and infinite appreciation to my supervisor **Felicia**. Thank you for all the time you put into my project. Thank you for observing process and success when I could not see it. Thank you for helping me think when my brain did not suffice on its own and thank you for helping me move forward when I got too involved in the details.

Abbreviations

ArtVen	Capillary network
ASD	Atrial septal defect
AV	Atrioventricular
IVC	Isovolumetric contraction
IVR	Isovolumetric relaxation
LA	Left atrium/atrial
LaLv	Mitral valve
LaRa	Atrial septal defect (model)
LAW	Left atrial wall
LV	Left ventricle/ventricular
LvRv	Ventricular septal defect (model)
LvSyArt	Aortic valve
LW	Left ventricular free wall
MRI	Magnetic resonance imaging
PDA	Patent ductus arteriosus
PuArt	Pulmonary artery
PuArtVen	Pulmonary capillary network
PuVen	Pulmonary vein
PuVenLa	Left atrial inflow
RA	Right atrium/atrial
RaRv	Tricuspid valve
RAW	Right atrial wall
RV	Right ventricle/ventricular
RvPuArt	Pulmonary valve
RW	Right ventricular free wall
SW	Septal wall
SyArt	Systemic artery
SyArtPuArt	Patent ductus arteriosus (model)
SyArtVen	Systemic capillary network
SyVen	Systemic vein
SyVenRa	Right atrial inflow
VSD	Ventricular septal defect

Chapter 1

Introduction

The human heart and the blood vessels constitutes the cardiovascular system, whose purpose is to provide organs and tissues of the body with oxygen and other essential substances and remove unessential metabolic products [1]. The group of disorders affecting the heart, blood vessels and conclusively the performance of the cardiovascular system is known as cardiovascular diseases and is the most common global cause of death annually [2]. In 2015, cardiovascular diseases accounted for 31.3% of all deaths [3].

Cardiovascular diseases are also the most common cause of death in Sweden [4]. Heart attacks, which is only one of many cardiovascular diseases, is the number one cause of death with 28 000 heart attacks occurring every year [5]. Known risk factors of heart diseases are physical inactivity, unhealthy diet, use of tobacco and harmful use of alcohol. Interventions on a population scale and on an individual scale may decrease the risk of suffering from a cardiovascular disease. It is believed that nearly 75% of recurrent vascular events may be prevented when executing interventions, such as cessation of tobacco use and treatment with medication. Identification of symptoms and individuals at high-risk are important to save lives [2]. The number of deaths in Sweden due to heart attacks have decreased with one third in the last 10 years thanks to research [5].

Anatomy and physiology can be studied using mathematics. Computer simulations can be used in an educational purpose to increase our knowledge in physiology. Simulations also make it possible to analyze the role different parameters play in the full scale model by changing parameters and testing various scenarios. Computer simulations of the cardiovascular system could therefore be an asset in cardiovascular understanding, diagnostics and treatment. Simulation models not only provide the possibility of studying the system in general, but also make it possible to model risk-factors and analyze how to attend specific situations to decrease the risk of cardiovascular diseases.

There are several existing models of the cardiovascular system. A few examples are Aplysia [6], the CircAdapt model [7] and SimVascular [8]. The focus of this

thesis will be on the CircAdapt model, that simulate beat-to-beat dynamics of the heart and blood vessels as a function of a large set of parameters and a small set of inputs from the user. The CircAdapt model and other simulation models are developed to provide simulations of the cardiovascular system, which often means that the model construction is a simplification of true anatomy and physiology.

Adapting cardiovascular simulation models to true heart geometry and cardiac pumping function would increase the range of which simulation models can be used for educational and clinical purposes. Accurate and valid cardiovascular models is a way of increasing our knowledge and improve diagnostics of cardiovascular diseases, without increasing the need of analysis directly on patients. Furthermore, improving physiological accuracy is an important step towards the goal of using cardiovascular modeling clinically with patient-specific data. Adapting and understanding existing cardiovascular simulation models is therefore an important field of study which require knowledge both in mathematical modeling as well as knowledge in anatomy and physiology.

Chapter 2

Theory

2.1 Anatomy and physiology of the cardiovascular system

An overview of cardiovascular physiology is described in Vander's Human Physiology [1]. Here the anatomy and physiology of the cardiovascular system will be presented in order to understand the project of modeling this system mathematically.

2.1.1 Cardiovascular system

The cardiovascular system, see Figure 2.1, act upon the body to supply organs and tissues with oxygen and other essential products as well as removing products such as metabolic end products. It is a closed system of two circuits, the pulmonary circulation and the systemic circulation.

The pulmonary circulation circulate from the right half of the heart, pumps deoxygenated blood through the lungs and returns oxygenated blood to the left half of the heart. The systemic circulation pumps oxygenated blood from the left half of the heart via the aorta to organs and tissues of the body and returns deoxygenated blood to the right half of the heart via the vena cava.

The heart is divided into a right half and a left half, both of which are composed longitudinally of two chambers. The upper chamber - the atrium - empties into the lower chamber - the ventricle - on the same side. The right ventricle empties into the pulmonary circulation and the left ventricle empties into the systemic circulation.

The blood vessels of the circulation belong to one of two categories; arteries and veins. Arteries carry blood away from the heart whereas veins return blood to the heart. The blood vessels are tube like structures that are all constructed of endothelial cells. Larger vessels also have layers of connective tissue and smooth muscle. Small arteries and small veins are connected via the capillaries; the location of oxygen exchange between blood and organs or tissues. The capillary network of the pulmonary circulation transport oxygen out of the lungs into the blood and the capillary network of the systemic circulation transport oxygen out of the blood into

organs and tissues. The exchange of oxygen and other nutrients in the capillaries is the ultimate function of the circulatory system. The blood flow in heart and blood vessels is made possible by pressure caused by the pumping action of the heart.

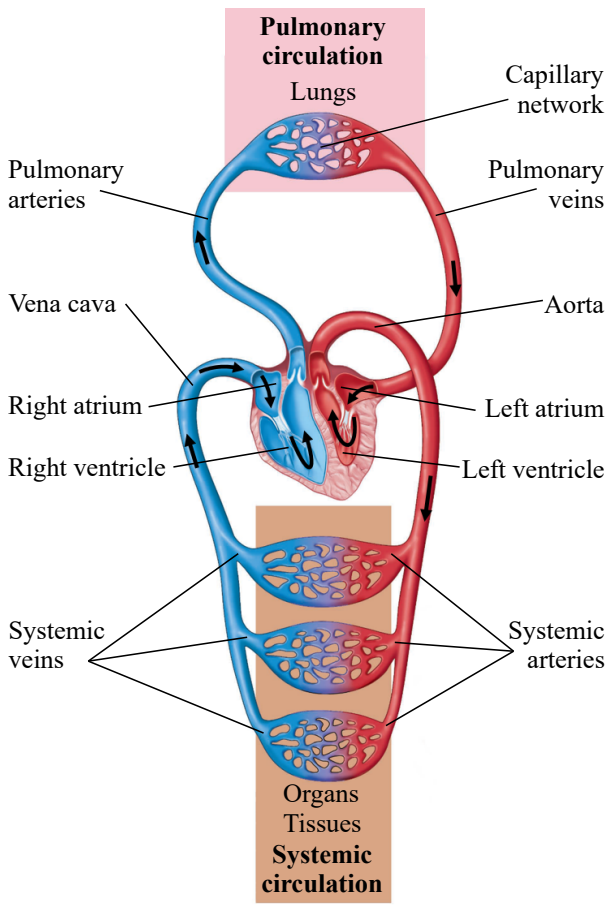

Figure 2.1: The cardiovascular system. The blue and red parts of the circulation represent deoxygenated blood and oxygenated blood respectively. The veins and arteries are simplified. Figure adapted from [1].

2.1.2 Heart anatomy

The heart anatomy and blood circulation through the heart is presented in Figure 2.2. The oxygenated blood returns to the heart from the lungs via the pulmonary veins to the left atrium. Separating the left atrium and ventricle is one of two atrioventricular (AV) valves - the mitral valve - permitting blood flow from the left atrium to the left ventricle. Blood flow from the left ventricle to the aorta and the systemic arteries is permitted by the aortic valve. The right side of the heart works in a similar

way by receiving blood from the systemic veins to the superior and inferior vena cava, into the right atrium. The blood flow from the right atrium through the second atrioventricular (AV) valve - the tricuspid valve - into the right ventricle and through the pulmonary valve to the pulmonary artery.

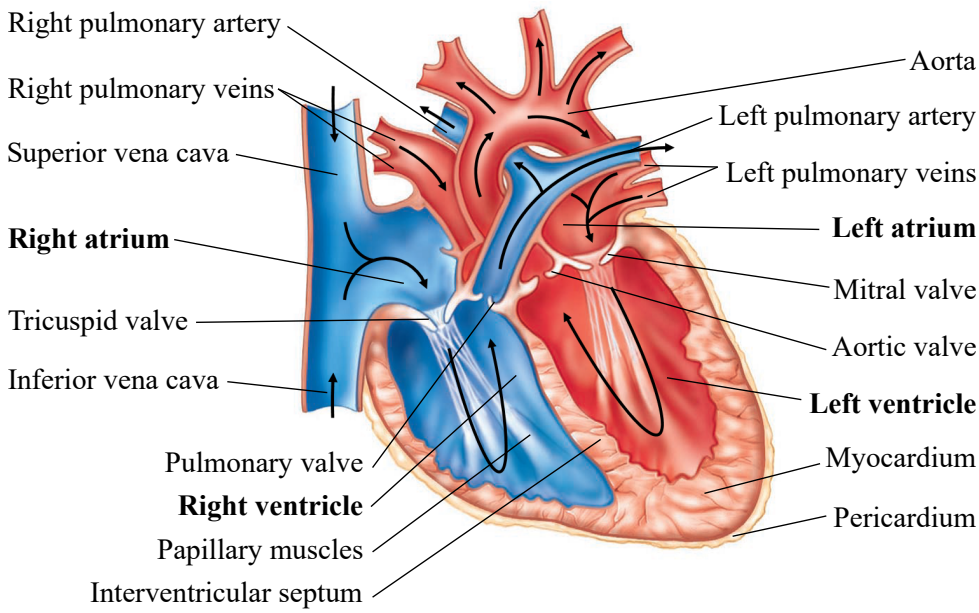

Figure 2.2: Human heart anatomy. The arrows show the direction of blood flow through the heart. Figure adapted from [1].

2.1.3 Valves

The opening and closing of the four valves are passive processes and are a result of flow and pressure differences across the valve. A closed valve is pushed open when the pressure in the cavity proximal to the valve, i.e. before the valve in the circulation, exceeds the pressure in the distal cavity, i.e after the valve in the circulation. A higher pressure in the atrium than in the corresponding ventricle push open the AV-valve. A higher pressure in the ventricle than in the aorta and pulmonary artery push open the aortic valve and the pulmonary valve. The valves are constructed to permit flow only from atrium to ventricle and from ventricle to corresponding artery and not backwards in the circulation.

When a valve is open there is very little resistance to flow, which permits large blood flows even to small pressure differences over the cavities. The rapid filling of the distal cavity result in an acceleration and moment of inertia that keeps the valve open for a period after the pressure gradient has changed direction. Only after the moment of inertia has decreased and the blood start to flow backward in the circulation, the valve is pushed closed [9]. Since the opening and closing of

the valves are passive processes, the AV-valves are connected to papillary muscles within the ventricles to avoid them pushing open into the atrium when the heart muscle contracts.

A damaged leaky valve is insufficient in stopping the blood flow when the valve is closed. A leaky valve, see Figure 2.3, allows blood flow backwards through the valve, causing turbulent flow, when the valve is closed. Even in healthy subjects, there is some leakage through the tricuspid valve and the mitral valve.

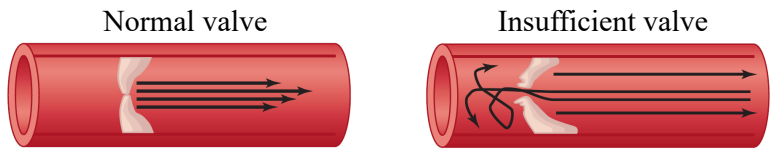

Figure 2.3: Figure demonstrating flow through a closed valve in the case of a normal valve (left figure) and an insufficient valve (right figure) [1].

2.1.4 Cardiac cycle - systole and diastole

The period of one heart beat is defined as one cardiac cycle. During the cardiac cycle, the left and right side of the heart work separately to contract the heart muscle and pump blood into the systemic and pulmonary circulation. For simplicity the assumption is made that the right and left side work simultaneously. In reality, there is a short delay between certain events in the right side cycle and the left side cycle of the heart due to effects of respiration. The cardiac cycle can be divided into two major phases; systole and diastole. These phases are based on current events of the ventricles. During systole the ventricle contracts and eject blood into the circulation. During diastole the ventricle relaxes and fills with blood from the atria. Both systole and diastole can be subdivided into two phases, see Figure 2.4.

The first part of systole is the isovolumetric contraction. The ventricles contract but all valves are closed, resulting in zero ventricular inflow and outflow of blood and a constant ventricular volume. The period of ventricular ejection during systole occur once the isovolumetric contraction has increased the ventricular pressure enough to overcome the pressure in the arteries. This push open the aortic and pulmonary valve, permitting blood flow to the aorta and pulmonary artery. During ejection the papillary muscles function to keep the AV-valves closed to avoid blood flow back into the atria. During ventricular ejection blood is forced into the arteries due to high ventricular pressure and a shortening of the heart muscle around the ventricles.

Isovolumetric relaxation of the ventricles during diastole involve closing of the aortic and pulmonary valves and ventricular relaxation. The AV-valves are also closed, resulting in zero flow in and out of the ventricles. The period of ventricular filling during diastole occur once the atrial pressure exceeds the ventricular pressure, pushing open the AV-valves permitting blood flow from atria to ventricle. During

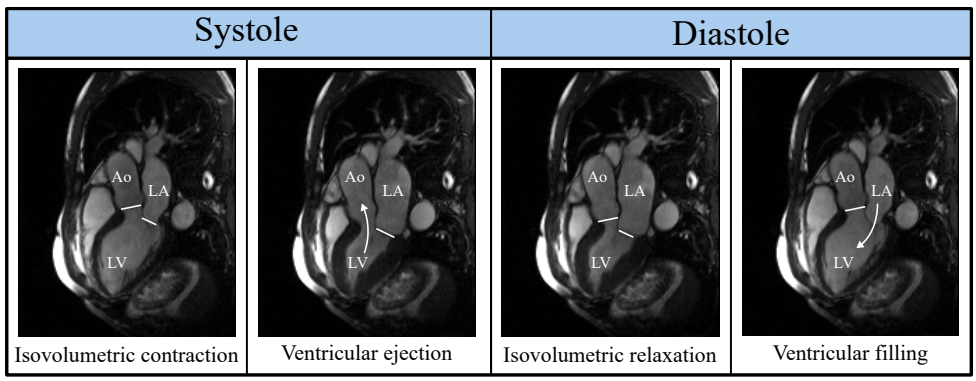

Figure 2.4: Cardiac cycle phases; systole and diastole. Each picture is a three chamber view taken at the end of each stage using MRI. The figure show the left atrium (LA), the left ventricle (LV) and the aorta (Ao). The lines and arrows depict closed valves and blood flow respectively. The course of event is similar for the right side of the heart.

the whole period of ventricular filling the pulmonary and aortic valves are closed and the ventricular heart muscle is relaxing. During the first part of ventricular filling, the cardiac muscle around the atrium is relaxed. This is known as the phase of early filling, where blood flow occur due to the built up pressure gradient across the AV-valves and a suction effect from the ventricles due to the low ventricular pressure and ventricular relaxation. After a period of ventricular filling the flow decreases, a period known as the diastasis. It is only during late stage of ventricular filling that the atria contracts, once again increasing the blood flow into the ventricle. Closing of the AV-valves complete the period of diastole.

2.1.5 Cardiac muscle and muscle contraction

The contraction and relaxation of the heart muscle during systole and diastole is what constitutes the pump function of the heart. Heart muscle, or cardiac muscle, is the tissue constituting the myocardium, see Figure 2.2, and is only found in the heart. The part of the myocardium called interventricular septum, or septal wall, separates the two ventricles from each other. The myocardium also consists of a left and right ventricular free wall and of cardiac muscle enclosing each atrium. The heart is enclosed within a fibrous, protective sac known as the pericardium. The pericardium is filled with a watery fluid that serves as a lubricant when the heart moves during contraction and relaxation of the cardiac muscle.

Cardiac muscle is constructed of single cardiac muscle cells, or muscle fibers, whose ends are connected to adjacent muscle cells. Each muscle fiber is constructed of myofibrils, see Figure 2.5. The myofibril is in its turn constructed of thick and thin filaments, see Figure 2.6, of cytosolic proteins. The filaments are organized within the myofibril in a parallel, repeating pattern. One junction of this repeating pattern is known as a sarcomere. The Z line define the limit of a sarcomere and

connects the thin filaments between two adjacent sarcomeres. Each sarcomere contains two sets of thin filaments, one side of the thin filament is anchored to the Z line whereas the other overlaps a small portion of the thick filaments. The thick filaments are located in the middle of a sarcomere and construct its A band.

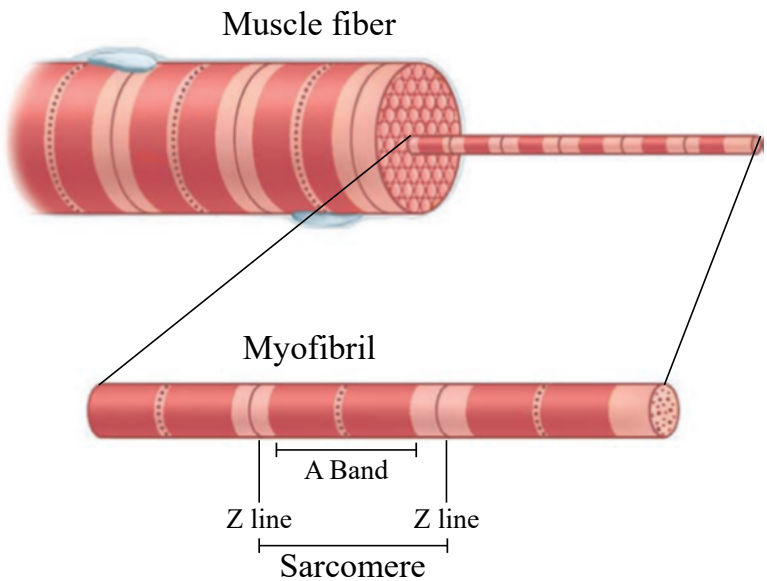

Figure 2.5: Cardiac muscle construction. Cardiac muscle is constructed of individual muscle fibers, constructed by myofibrils. Each myofibril is constructed of a repeating pattern of sarcomeres. Figure adapted from [1].

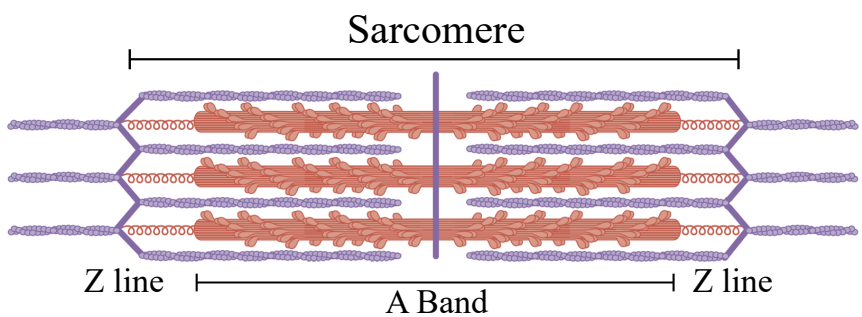

Figure 2.6: Sarcomere construction. Sarcomeres are constructed of a parallel pattern of thick filaments (brown units) and thin filaments (purple units). Figure adapted from [1].

Cardiac muscle contraction occur due to a shortening of the sarcomeres, resulting in a shortening of the cardiac muscle. Shortening of the sarcomeres is made possible by action potentials triggering the myocardium, causing the thick and thin filaments to bind to each other. This binding, known as cross-bridge formation, oc-

cur as long as action potentials affect the area of cardiac muscle and result in the filaments sliding past each other. This movement result in a shortening of each sarcomere, but not in the filaments themselves, see Figure 2.7. An absence of action potentials prevent further shortening and relaxes the sarcomeres. Shortening and relaxing of sarcomeres due to the presence and absence of action potentials is the physiology of contraction and relaxation of the heart muscle.

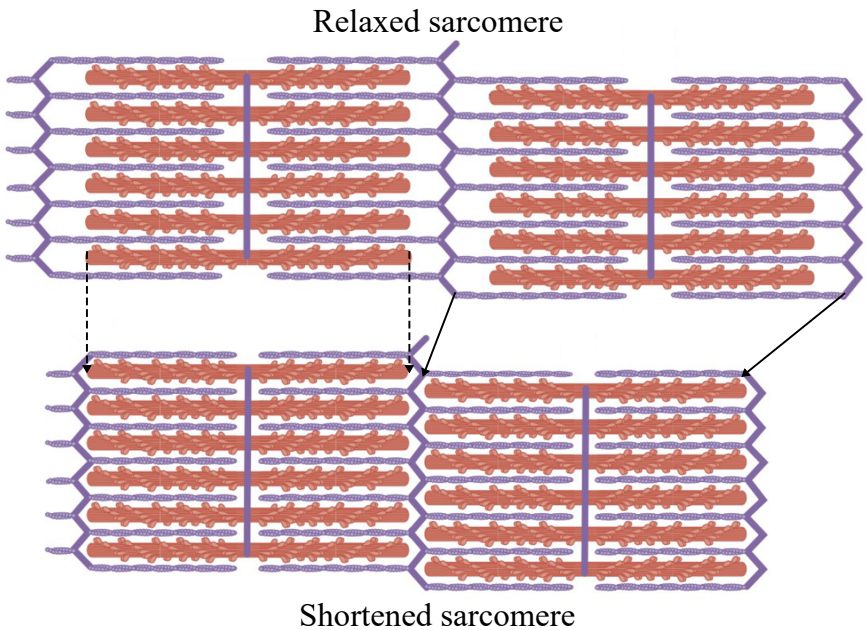

Figure 2.7: Sarcomere contraction. Notice the unchanged A band length (dashed lines) and the shortened distance between the Z lines (continuous lines). Figure adapted from [1].

2.1.6 Radial and longitudinal pumping

The myocardium, constructed by cardiac muscle, is naturally constant in volume throughout the cardiac cycle. The blood volume in each heart chamber however, vary over time. One can define the total heart volume as the total volume enclosed within the outer boundary of the myocardium. To understand the variation of the total heart volume throughout the cardiac cycle, the physiology of cardiac muscle contraction is analyzed using MR-images, see Figure 2.8. From these images one can identify the total heart volume as the outer boundary of cardiac muscle, delineated for diastole as the red dashed line and for systole as the blue dashed line. One can also identify the AV-plane as the line between atria and ventricles through the AV-valves, delineated for diastole as the white dashed line and for systole as the white continuous line. As can be seen from the images, the outer volume change throughout the cardiac cycle has not changed significantly whereas there is a significant displacement of the AV-plane between systole and diastole. The reason for

this can be explained by further analysis of the mechanism of cardiac pumping.

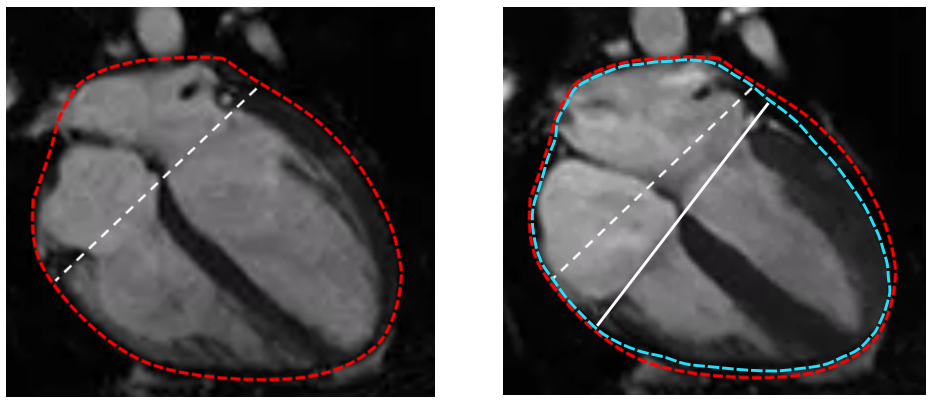

Figure 2.8: Four chamber view of the heart by MRI. The left and right panel show the heart in end diastole and end systole respectively. Total heart volume is depicted at end diastole (left panel, red dashed line) and at end systole (right panel, blue dashed line). As is the AV-plane in end diastole (left panel, white dashed line) and end systole (right panel, white line). Comparing diastole to systole it can be seen that there is a small decrease in total heart volume and a large displacement of the AV-plane.

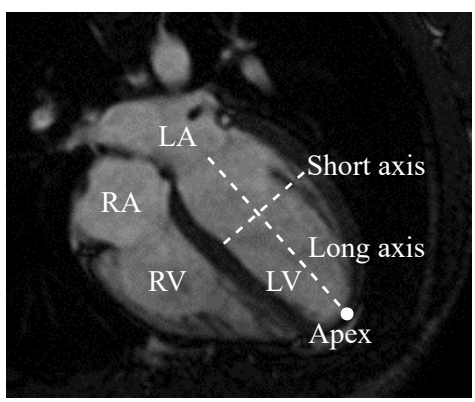

Figure 2.9: Four chamber view of the heart using MRI. The short axis and long axis are shown as dashed lines in relation to right (RA) and left (LA) atria and right (RV) and left (LV) ventricle. Apex of the heart is depicted by the white dot. The image show the heart at end diastole.

The pumping function of the heart can be divided into two components of ventricular pump function; radial pumping and longitudinal pumping. Radial pumping is defined as the pumping caused by a contraction along the short axis of the heart, see Figure 2.9, which acts as a squeezing motion of the heart affecting the total heart volume. Longitudinal pumping is defined as the contraction along the long axis, which result in a displacement of the AV-plane towards the apex without contributing to the variation of the hearts total volume [10].

Studies using MRI suggest that the total heart volume variation in healthy subjects is approximately 8% and in the range 5-11% throughout the cardiac cycle [11]. As radial pumping is the only component of ventricular contraction contributing to this variation, this result suggest that a large portion of the pumping mechanism and heart function is due to longitudinal contraction and a displacement of the AV-plane. Longitudinal pumping have shown to be an important mechanism in heart pumping efficiency. A large total heart volume variation will result in

energy loss during the cardiac cycle [10]. Recent studies have also shown that a reduced function in left ventricular longitudinal pumping is an independent predictor of major adverse cardiac events [12].

2.1.7 Septal defects and patent ductus arteriosus

A septal defect is a defect in the myocardium, resulting in a small hole in the septal wall. An atrial septal defect (ASD) allows blood flow between the two atria. Similarly, a ventricular septal defect (VSD) permits blood flow between the right and left ventricle [1].

Patent ductus arteriosus (PDA) is a congenital heart defect allowing blood flow between the aorta and the pulmonary artery. Before birth these two arteries are connected by a small blood vessel that normally closes short after birth. In PDA patients this vessel remains open, resulting in abnormal blood flow from the aorta to the pulmonary artery [13].

2.1.8 Summation of a heart beat

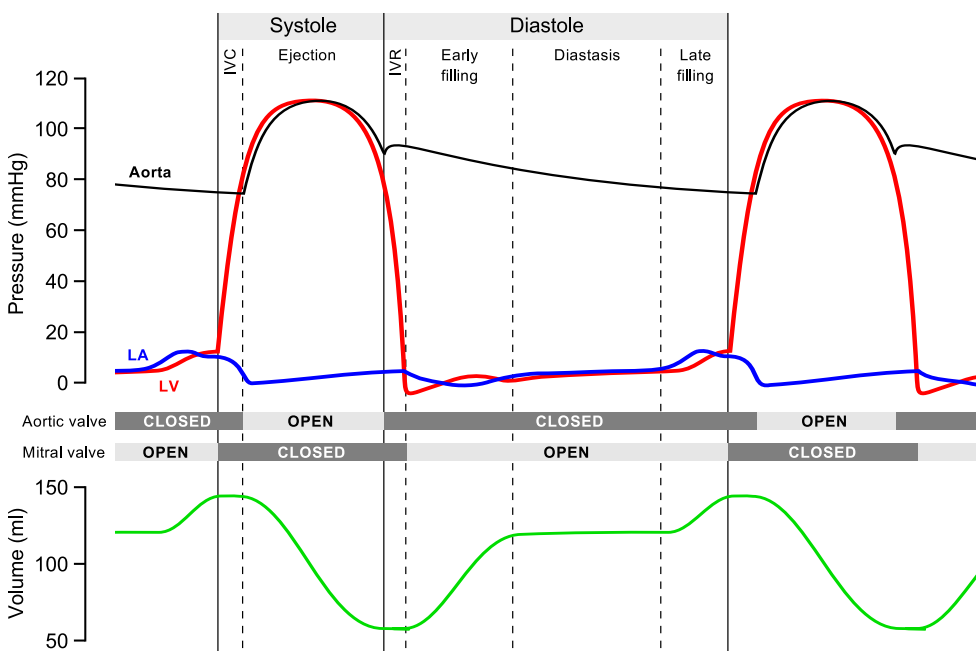

Figure 2.10: Wigger diagram describing the cardiac cycle [14]. The diagram align pressure and volume throughout the cardiac cycle. The pressure curve show aortic pressure (black line), left ventricular pressure (red line) and left atrial pressure (blue line). The volume show the left ventricular volume (green line).

Previously presented theory can now be summarized to describe one complete heart beat. A description of events and physical properties of the heart throughout the cardiac cycle can be illustrated by the Wigger diagram, see Figure 2.10. The ventricular myocardial wall start to contract during isovolumetric contraction (IVC). Due to blood being essentially incompressible and an increasing pressure in the ventricle, the ventricular cardiac muscle develop tension in the sarcomeres but does not shorten. When the pressure in the ventricles exceed the pressure in the aorta and pulmonary artery, the pressure difference push open the aortic and pulmonary valve. This leads to ventricular ejection, where a shortening of the ventricular muscle occur and blood flow from ventricles to arteries. At the same time the blood volume of the atria increase due to the longitudinal displacement of the AV-plane towards the apex. Once the pressure in the arteries exceed the ventricular pressure the arterial blood decelerates and the valves close. During isovolumetric relaxation (IVR) the sarcomere shortening cease, the ventricular cardiac muscle relaxes and all valves are once again closed. The atria are continuously filled with blood from the veins. The AV-valves are pushed open when the blood pressure increasing in the atrium exceed the ventricular pressure, causing ventricular filling. The period of rapid filling due to the pressure difference and displacement of the AV-plane is followed by the diastasis where the ventricular volume is approximately constant. Following the diastasis is sarcomere shortening of the atrial walls, causing atrial muscle contraction and additional filling of the ventricles. When the ventricular pressure exceed the atrial pressure, the AV-valves are pushed close and the cardiac cycle is complete.

2.2 Cardiac physiology as a physical model

$$\Delta P = Q \cdot R$$

Pressure	P	Pressure is defined as the force acting on a surface by an object. Modeling the cardiovascular system, blood pressure is used as a measurement of the force of which the blood pushes on its surrounding walls as it is enclosed within heart chambers and blood vessels.
Flow	Q	The blood flow is defined as the movement of blood in heart and vessels and through valves and capillary networks. Blood flow is measured as volume over time and is directly proportional to the pressure difference between two points in the blood filled cavities.

Resistance	R	Resistance is defined as the opposition to movement. In cardiovascular modeling, resistance is used to model opposition to blood flow in blood vessels and heart chambers. Here the resistance is proportional to the blood viscosity, cross-section area and length of the cavity [1].

$$T=\mathbf{f}(\sigma), \quad \sigma = \mathbf{g}(\varepsilon)$$

Tension	T	Tension is defined as the force exerted on an object by a contracting muscle [1]. During contraction the cardiac muscle of the myocardial walls develop tension as a function f of the sarcomere shortening, which act upon the blood in the heart.
Strain	ε	The relative length change of av object subject to an applied force is known as the strain [15]. The sarcomeres of the heart muscle develop strain during sarcomere shortening and myocardial contraction.
Stress	σ	Stress developing in an object is given by the applied force over the applied area [15]. Myocardial contraction not only shorten the sarcomeres but naturally develop stress in the thin filaments in the process. The stress-strain relationship in cardiac muscle sarcomeres is a function g determined by material properties.

2.3 CircAdapt

The CircAdapt model is a mathematical simulation model implemented to simulate beat-to-beat dynamics of the cardiovascular system. The model aims to facilitate education and research of cardiovascular physiology and can be downloaded free of charge from the CircAdapt website [7]. The website enables download of both the CircAdapt Simulator and the CircAdapt MATLAB source code. This thesis project will focus on analysis and adaptation of the CircAdapt source code. The CircAdapt model is developed by the CircAdapt Research Team based at the Department of Biomedical Engineering at Maastricht University in The Netherlands.

The construction of the model is presented in the CircAdapt Simulator manual [16] and in the CircAdapt article published by Lumens et al [17]. Other tools for understanding the model are the source code itself [18] and the CircAdapt source code manual [19]. A schematic figure of the model is presented in Figure 2.11.

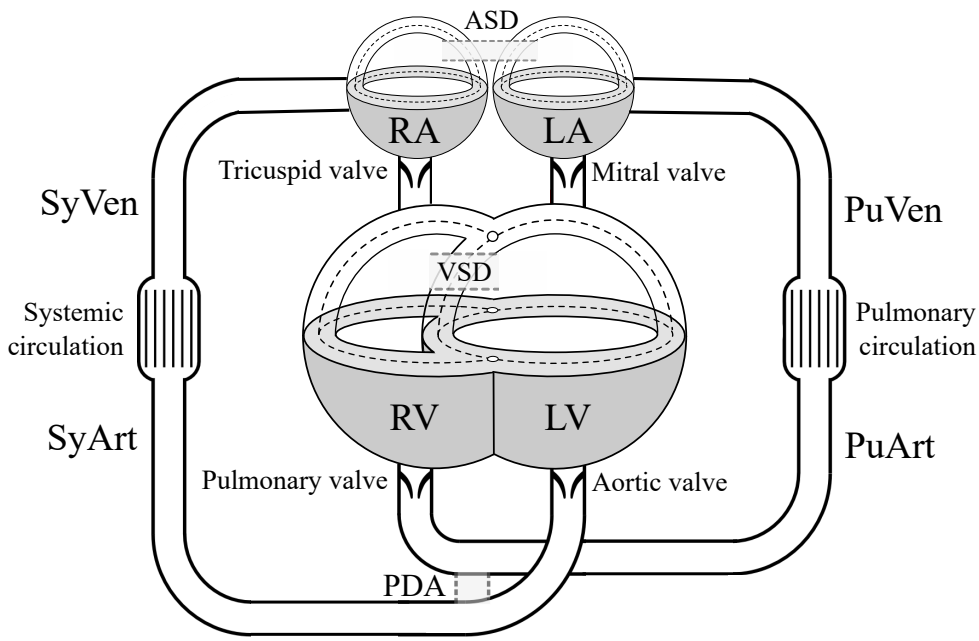

Figure 2.11: A schematic presentation of the CircAdapt model. The model represent the left atrium (LA) and right atrium (RA) as spherical cavities and the left ventricle (LV) and right ventricle (RV) as a three-wall spherical segment. The model includes four blood vessels; systemic artery (SyArt), systemic vein (SyVen), pulmonary artery (PuArt) and pulmonary vein (PuVen). Possible abnormalities, such as atrial septal defect (ASD), ventricular septal defect (VSD) and patent ductus arteriosus (PDA) are also presented. Figure adapted from [16].

2.3.1 Arteries and veins

Arteries and veins are modeled as non-linear, elastic tubes with blood enclosed by a vessel wall. The model is restricted to modeling the two circulations as four vessels; systemic artery (SyArt), systemic vein (SyVen), pulmonary artery (PuArt) and pulmonary vein (PuVen).

2.3.2 Heart and pericardium

The four heart chambers are modeled as three separate components. The right atrium (RA) and the left atrium (LA) are modeled as spherical cavities of blood enclosed by a single myocardial wall; the left atrial wall (LAW) and the right atrial wall (RAW). The left (LV) and right (RV) ventricles are modeled as a three-wall segment where the two ventricular blood filled cavities are enclosed by three myocardial walls. The ventricles are enclosed by the left ventricular free wall (LW) and the right ventricular free wall (RW) and separated by the septal wall (SW). All chambers of the heart are simplified to be segments of spherical cavities. The peri-

cardium is modeled as a thin bag, with no cavity of its own, enclosing all heart components.

2.3.3 Patches and myocardial contraction

The pump function of the heart is modeled by dividing each of the five myocardial walls into a fixed number of patches. The cardiac muscle contraction is then simulated by modeling sarcomere mechanics of each patch. The original CircAdapt model is limited to five patches, one for each wall. As the heart cavities are modeled as spherical segments, the CircAdapt model is based solely on radial pumping of the heart.

2.3.4 Cavity nodes, valves and capillary networks

The CircAdapt model construct a closed-loop circulation by connecting each blood filled cavity, blood vessels and heart chambers, to its adjacent valves or capillary networks. There are nine flow channels modeled as valves in the original CircAdapt model. The tricuspid valve (RaRv), the pulmonary valve (RvPuArt), the mitral valve (LaLv) and the aortic valve (LvSyArt) are the only true valves of the model. Right atrial inflow (SyVenRa) and left atrial inflow (PuVenLa) as well as the three shunts ASD (LaRa), VSD (LvRv) and PDA (SyArtPuArt) are also modeled as valves. The model includes two capillary networks; the systemic capillary network (SyArtVen) and the pulmonary capillary network (PuArtVen).

Chapter 3

Aim

The first part of this thesis project is a literature study in cardiovascular physiology and in the CircAdapt cardiovascular simulation model. The second part of the thesis is to apply the knowledge from this literature study to improve the model.

The specific aims of the thesis are to,

- Study the CircAdapt model construction and execution and derive the implemented equations.
- Identify the model limitations in regard to cardiovascular anatomy and physiology.
- Adapt the model to improve its accuracy in the physiological aspect of radial and longitudinal pumping.

Chapter 4

Original CircAdapt model

The original CircAdapt model is in this thesis analyzed according to its MATLAB source code [18]. A graphical representation of the model execution using the model main file can be found in Figure 4.1.

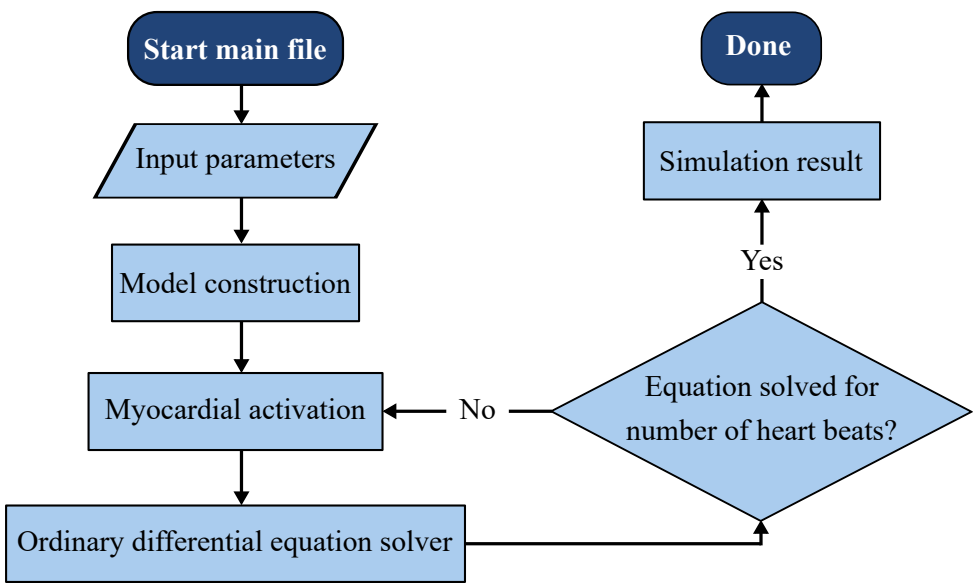

Figure 4.1: Flow chart of the original CircAdapt simulation model. The source code running the simulation is implemented in MATLAB.

Execution of the simulation starts with the user entering four input parameters, after which a model structure representing the cardiovascular system is constructed. The myocardial activation, contraction and relaxation throughout the cardiac cycle is determined and a single heart beat is simulated using an ordinary differential equation solver. This is repeated for the same structure until the correct number of heart beats are simulated. The result of the simulation can be accessed by the user

and is depicted as a plot of the simulated hemodynamics for all heart beats. The execution procedure is described in more detail for each box of the flow chart in the following sections.

4.1 Input parameters

The CircAdapt model is executed for a small set of input parameters entered by the user, see Table 4.1. The user can start the simulation based on default values or choose to change one or several of the input parameter values. The default values of the input parameters are presented in Table A.1 in Appendix A.1.

NOTATION	INPUT PARAMETER DESCRIPTION
p_0	**Mean arterial pressure**. The average blood pressure during a cardiac cycle.
q_0	**Cardiac output**. The blood flow from the left ventricle to the systemic circulation.
N_{HB}	**Number of heart beats**. The number of heart beats, i.e. cardiac cycles to be simulated.
t_{CC}	**Cardiac cycle time**. The duration of one cardiac cycle.

Table 4.1: Input parameters of the original CircAdapt model. The default values of the parameters are presented in Table A.1 in Appendix A.1.

4.2 Model construction

Running the CircAdapt model automatically constructs a structure representing the cardiovascular system. This structure, presented in Section 2.3, is constructed of blood filled enclosed cavities, walls of cardiac muscle surrounding the heart cavities, a pericardium, valves and capillary networks of the systemic and pulmonary circulation.

The model structure include approximately 150 parameters, including the four input parameters set by the user. Model parameters are defined as material properties or physiological constants whose values are fixed throughout the simulation. The parameter values of the original CircAdapt model are presented in Appendix A.1.

The model structure also include approximately 250 variables. The variables of the model include all dynamical properties of the cardiovascular system, varying throughout the cardiac cycle. Out of the 250 variables, only 30 are considered as state variables, see Table 4.2. The state variables are the only variables used directly

by the ordinary differential equation solver to track the dynamics of the cardiac cycle. They are consequently the only variables that are given initial values, see Table A.10 in Appendix A.2, which correspond to the initial state of the simulation. The initial state of the system is at the end of the diastasis, in diastole, of the cardiac cycle.

NOTATION	STATE VARIABLE DESCRIPTION
t	**Time**. The time variable keeps track of the current time and range from the start time to the end time of the cardiac cycle. There is **1** time variable.
V	**Cavity Volume**. The blood volume of each cavity at each time step. There are **8** cavities included in the model.
q	**Valve flow**. The flow through each model valve at each time step. The model includes **9** "valves".
C	**Contractility**. The density of cross-bridge formation in a muscle patch over time. The model includes one contractility variable for each myocardial wall patch, consequently **5** contractility variables.
L_{si}	**Intrinsic sarcomere length**. The intrinsic length of the sarcomeres in a muscle patch at each time. There are **5** sarcomere length variables, one for each wall patch.
$V_{m,SW}$	**Septal midwall volume**. The midwall volume of the ventricular septal wall at each time step. Will be introduced in detail in Section 4.4.3. There is **1** midwall volume variable.
y_m	**Junction radius**. The radius of the circular sphere-sphere intersection of the ventricular three-wall segment. Will be introduced in detail in Section 4.4.3. There is **1** junction radius variable.

Table 4.2: State variables of the CircAdapt model. The initial values are presented in Appendix A.2.

4.3 Myocardial activation

A single cardiac cycle is modeled using mechanics of the heart muscle. Recalling the background theory of the cardiac cycle, the cardiac muscle surrounding atria and ventricles undergoes contraction and relaxation during a cycle. The cardiac muscle contraction is modeled by determining activation and contraction duration in the sarcomeres of each muscle patch of the model. As the original model uses one patch per cardiac muscle wall, the contraction is uniform throughout the wall.

The model defines the starting time of a cardiac cycle as the time point t_{RAW} where the contraction of the right atrial wall is activated due to actions potentials. This is a reasonable assumption to make since the activation of the heart normally start by an activation of the cardiac muscle around the right atrium, close to the superior vena cava [1]. The time of the activation of the left atrial wall, t_{LAW}, occur a short time after the right atrium. The right ventricular free wall starts contracting at time t_{RW}, after both the right and the left atrial wall. The activation time of the septal wall t_{SW} and the left ventricular free wall t_{LW} are set to the same time as the right free wall. These approximations are reasonable since there is a delay between atrial and ventricular contraction and since the ventricular walls contract nearly simultaneously [1]. For a graphical representation of the myocardial activation pattern for the first cardiac cycle, see Figure 4.2.

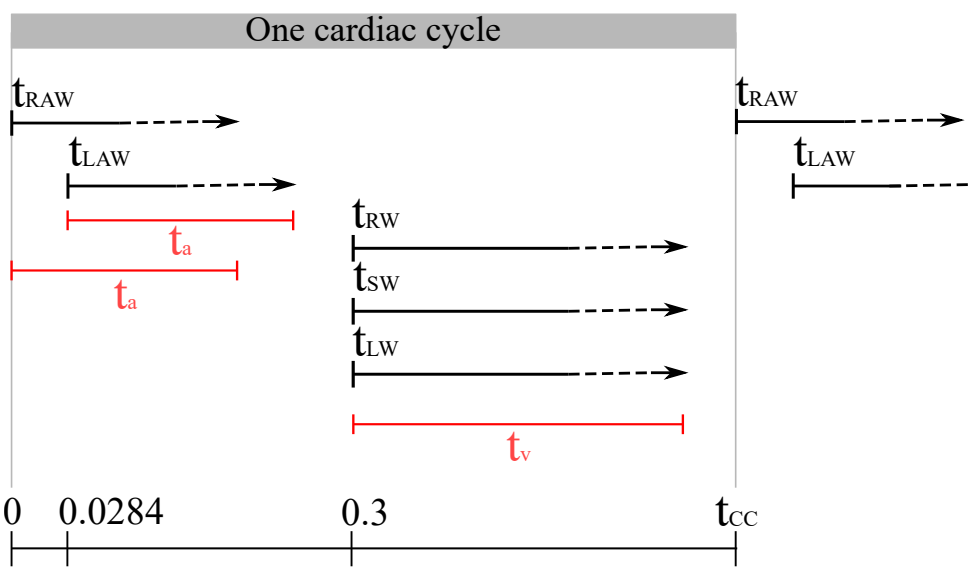

Figure 4.2: Activation pattern of the myocardial walls throughout the first cardiac cycle. t_{RAW}, t_{LAW}, t_{RW}, t_{SW} and t_{LW} are the times of contraction activation due to action potentials for each model wall. t_a and t_v are the contraction duration of the atria and ventricle respectively. t_{CC} is the duration of one cardiac cycle input by the user.

The delay between each contraction activation is given by the values,

$$
\begin{aligned}
t_{RAW} &= 0 && (4.1)\\
t_{LAW} - t_{RAW} &= 0.0284 && (4.2)\\
t_{RW} - t_{RAW} &= 2\tau_{AV} && (4.3)\\
t_{SW} - t_{RAW} &= 2\tau_{AV} && (4.4)\\
t_{LW} - t_{RAW} &= 2\tau_{AV}. && (4.5)
\end{aligned}
$$

The time constant τ_{AV} depict the time delay between right atrial and right ventricular activation and is determined as,

$$
\tau_{AV} = \begin{cases} 0.15 & \text{for the first heart beat} \\ 0.1765 t_{CC} & \text{for succeeding heart beats.} \end{cases} \tag{4.6}
$$

The time between two succeeding activations of the right atrium is set equal to the duration time of one complete cardiac cycle t_{CC} expressed in seconds.

The contraction duration of each wall is determined as a fraction of the cardiac cycle time, t_{CC}. There are two time constants of contraction duration, one determining the contraction of the atrium t_a and one determining the contraction of the ventricle t_v. The two duration constants are calculated as,

$$
\begin{aligned}
t_a &= 0.1765 t_{CC} && (4.7)\\
t_v &= 0.085 + 0.4 t_{CC} && (4.8)
\end{aligned}
$$

where t_{CC} is the cardiac cycle time expressed in seconds.

4.4 Ordinary differential equation solver

The dynamic properties of the cardiovascular system are determined beat-by-beat as a system of ordinary differential equations. The system is solved using an ordinary differential equation solver. The solver used is $ode113$, which is a nonstiff, built in MATLAB-solver constructed to solve ordinary differential equations. It solves the dynamic over time using a time vector, initial values of the system variables and a MATLAB-function depicting the system of differential equations.

The time vector is constructed as a vector from start time to end time of a cardiac cycle t_{CC} with a time step length dt, see Table A.1. The initial values are in this case initial values of the state variables, see Table 4.2. The initial values of the first simulated heart beat are presented in Table A.10. The initial values of succeeding heart beats are the state variable values of the last time step $t = t_{CC}$ of the preceding heart beat.

A flow chart of the MATLAB-function depicting the ordinary differential equation system is presented in Figure 4.3. The function include several inner functions,

all together constructing a model of the cardiovascular system. All functions within the flow chart are called for each time step until the cardiac cycle is complete. The input to each time step are the state variables. The output of each complete time step is the state variable derivatives. Available throughout the simulation are the structure parameters, see Appendix A.1. The execution of each inner function of the flow chart is described in detail in the following subsections.

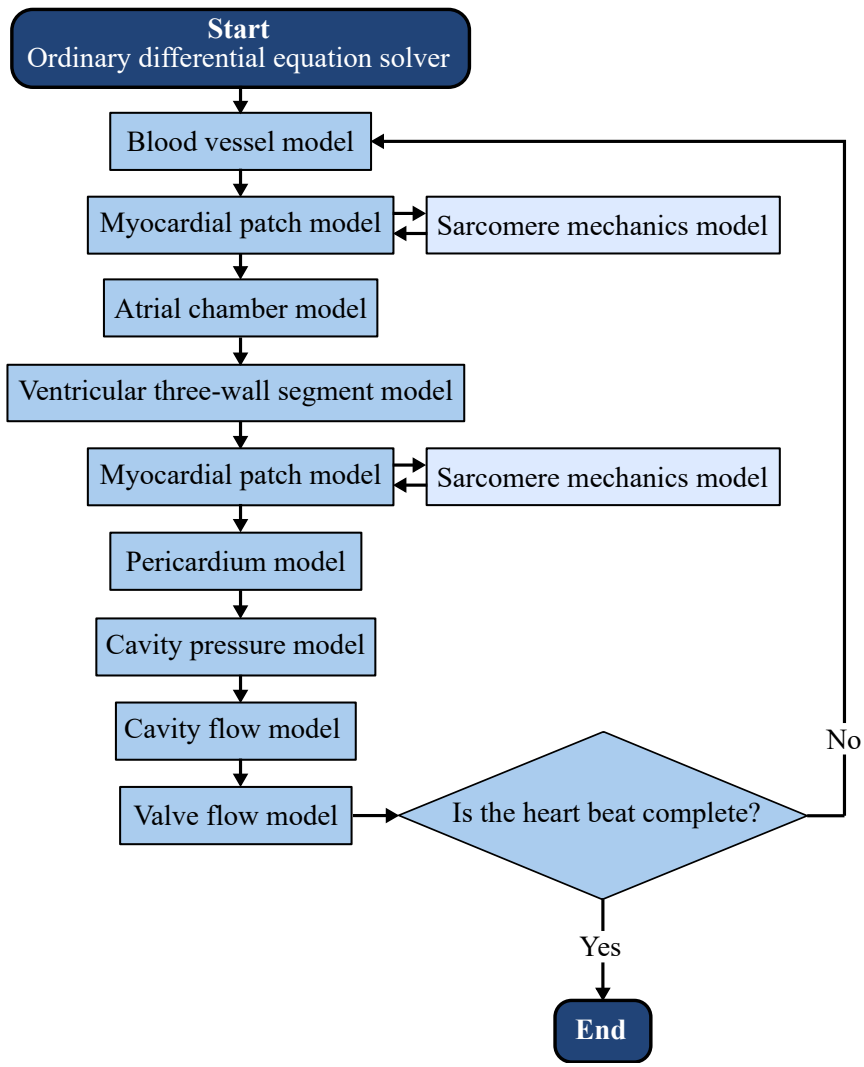

Figure 4.3: Flow chart of the MATLAB-function used within the ordinary differential equation solver *ode*113. A description of each inner function is presented in upcoming subsections.

4.4.1 Blood vessel model

The blood vessel model implements arteries and veins as an electric circuit with resistance, blood pressure and blood flow. A geometrical representation of the blood vessel model can be seen in Figure 4.4. Do recall the simplification of the CircAdapt model that limits the analysis to four blood vessels; systemic artery, systemic vein, pulmonary artery and pulmonary vein. The implementation of modeling the four blood vessels is described in the article of blood vessel simulation by Arts et al. [20] and in the source code of the CircAdapt model [18].

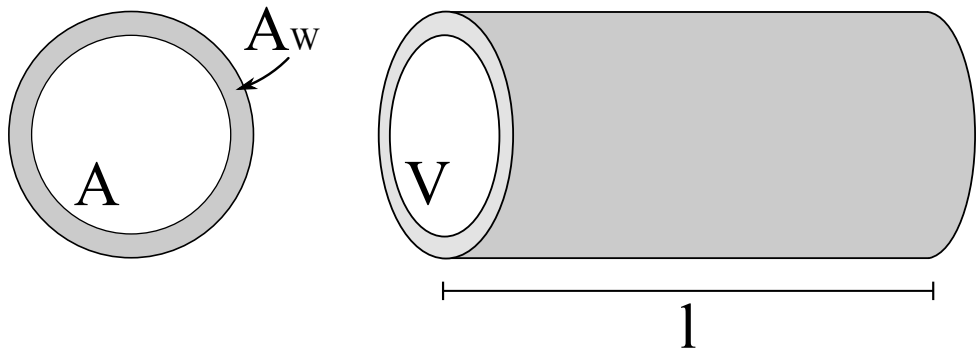

Figure 4.4: The blood vessel model. To the left is a cross-section, two dimensional image of the blood vessel with cavity blood cross-section area A and wall cross-section area A_W. To the right is a three dimensional figure of the vessel with cavity blood volume V and vessel length l.

The CircAdapt model uses an adaptation of a classic electrical circuit model, modeling vessel resistance, to create a circuit model whose elements are more closely related to true physical properties of the blood vessels. Recalling that most blood vessel walls are constructed of smooth muscle and connective tissue, the material properties of the wall can be considered non-linearly elastic. This non-linearity is represented by an exponential relation between the stress and the strain of the cardiac wall fibers. Assuming a thin wall, mean fiber stress and strain are related to cavity pressure and ratio of cavity to wall cross-section area A/A_W, see Figure 4.4. Using this relation, Arts et al. derive the transmural pressure p_W across the vessel wall as,

$$p_W = p_{Ref}\left(\frac{A/A_W + 0.5}{A_{Ref}/A_W + 0.5}\right)^{\frac{k}{3}-1} \tag{4.9}$$

where the parameters p_{Ref} is the reference pressure at reference cavity cross-section area A_{Ref}. k is the wall fiber stiffness and A_W is the cross-section area of the wall. A is the cavity cross-section area calculated as

$$A = \frac{V}{l}. \tag{4.10}$$

Here V is the state variable cavity blood volume and l is the vessel length parameter. The values of all blood vessel parameters for all four blood vessels can be found in Table A.2. The transmural pressure p_W will be used later on to calculate the blood pressure within the blood vessel cavity.

The relation between pressure and flow in a blood vessel is based on wall elastic properties, blood vessel size, blood viscosity and vessel resistance [15]. In the CircAdapt model, resistance in blood filled cavities due to hemodynamics is modeled as wave impedance, Z. For the CircAdapt model, assuming large vessels, the viscous effects can be neglected [15] and the wave impedance Z can be derived from blood inertia and compliance and calculated as,

$$Z = \sqrt{\frac{p_W \rho (k/3 - 1)}{A(A + 0.5A_W)}} \tag{4.11}$$

where ρ is the blood density stated in Table A.1. For the proof of this see Appendix B.1. The wave impedance Z will be used later on to calculate blood flow through the vessels.

4.4.2 Atrial chamber model

The atrium is modeled using the chamber model. A chamber is defined and modeled as a spherical cavity with blood, surrounded by a single myocardial wall. The chamber model is described in theory in the article by Arts et al. describing the CircAdapt model [17] and the execution of the model is described in the source code [18]. Each atrium is a chamber segment of the full CircAdapt model, see Figure 4.5. Thus, the left atrium has a cavity blood volume V_{LA} and a myocardial wall volume V_{LAW} and the right atrium has a cavity blood volume V_{RA} and a myocardial wall volume V_{RAW}.

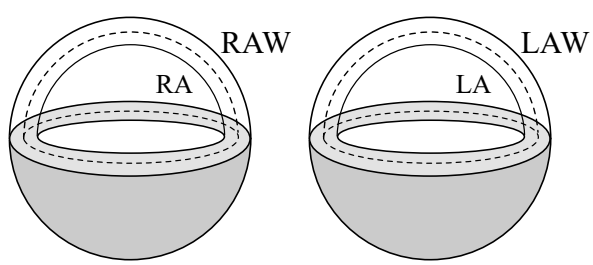

Figure 4.5: The atrial chamber model of the CircAdapt model. The left and right atria are represented as two separate spheres. The left atrial blood volume (LA) is enclosed by a left atrial myocardial wall (LAW). Similarily the right atrium blood volume (RA) is enclosed by a right atrial myocardial wall (RAW). Figure adapted from [21].

The chamber model determines tension and transmural pressure of the atrial walls and blood flow resistance of the atrial cavities. The cavity volume, see Figure

4.6, is equal to the blood volume of the atrium and is a state variable varying over time as a result of the myocardial contraction and relaxation. The wall volume is a parameter whose values are presented in Table A.3.

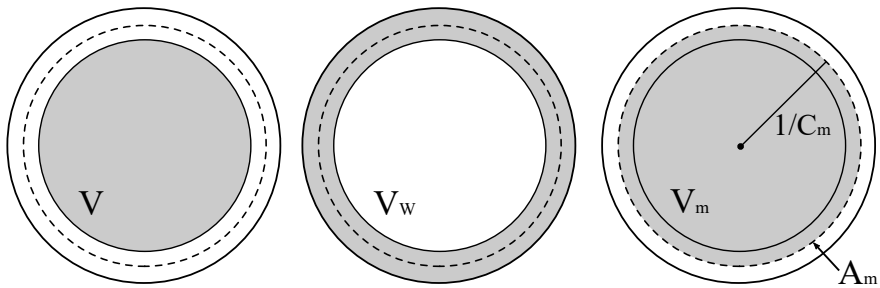

Figure 4.6: Cross-sections of the chamber model. The grey area depict the cavity volume V (left panel), the wall volume V_W (middle panel) and the midwall volume V_m (right panel). The right panel also show the defined midwall curvature C_m and midwall surface are A_m.

The midwall surface of a chamber segment is defined as the spherical surface that divides the wall volume V_W in an inner and outer shell of equal volume [21]. Further the midwall volume V_m, see Figure 4.6, is defined as the volume enclosed by the midwall surface [21]. By this definition the midwall volume of the left atrium $V_{m,LA}$ and the right atrium $V_{m,RA}$ can be calculated as,

$$V_{m,LA} = V_{LA} + \frac{V_{LAW}}{2} \tag{4.12}$$

$$V_{m,RA} = V_{RA} + \frac{V_{RAW}}{2}. \tag{4.13}$$

It also follows from Figure 4.6 geometry that the midwall curvature C_m (the inverse of the midwall radius) and midwall surface area A_m can be calculated from the midwall volume V_m of each atrium as,

$$C_m = \left(\frac{4\pi}{3V_m}\right)^{1/3} \tag{4.14}$$

$$A_m = \frac{4\pi}{C_m^2}. \tag{4.15}$$

Using Equation (4.15), the wall tension T_m is defined as,

$$T_m = \frac{dT}{dA}(A_m - A_{m0}) \tag{4.16}$$

where A_{m0} is the midwall surface area at zero tension and dT/dA is the wall area stiffness, which both depend on the myocardial contraction of the wall for each time step. The tension T_m will be used further on to model sarcomere contraction

of the myocardial walls. The transmural pressure p_W over the atrial wall can now be calculated using spherical geometry and conservation of energy [21] as,

$$p_W = 2C_m T_m. \tag{4.17}$$

The transmural pressure will be used later on to calculate the blood pressure within the chamber cavity.

Similarly to the blood vessel model, the cavity wave impedance Z of the atria is calculated as a measurement of resistance, i.e. opposition to blood flow. The cross-section area of the left A_{LA} and right A_{RA} atria are estimated as,

$$\begin{cases} A_{LA} &= \dfrac{V_{LA} + 0.1V_{LAW}}{2(V_{m,LA})^{1/3}} \\ A_{RA} &= \dfrac{V_{RA} + 0.1V_{RAW}}{2(V_{m,RA})^{1/3}}. \end{cases} \tag{4.18}$$

and the wave impedance of the left Z_{LA} and right Z_{RA} atrium are calculated as,

$$\begin{cases} Z_{LA} &= \dfrac{0.2\sqrt{2\rho(V_{m,LA})^{1/3}\left|\dfrac{dT}{dA}\right|}}{A_{LA}} \\ Z_{RA} &= \dfrac{0.2\sqrt{2\rho(V_{m,RA})^{1/3}\left|\dfrac{dT}{dA}\right|}}{A_{RA}}. \end{cases} \tag{4.19}$$

The impedance will be used later on to calculate blood flow through the atrium.

4.4.3 Ventricular three-wall segment model

The three-wall segment models the ventricles of the heart as mechanical interaction between the left and right ventricular blood volume and the surrounding myocardium. The model determines wall tension and transmural pressure of the three walls and wave impedance of the two cavities. The construction of the three-wall segment and its implementation is described in the three-wall segment article by Lumens et al. [21] and in the simulator manual [16]. The execution of the model is described in the source code [18].

The three-wall segment model construct the ventricles as a conjoint segment. The left ventricular blood volume V_{LV} and the right ventricular blood volume V_{RV} are separated by the septal wall V_{SW} and encapsulated within the left ventricular free wall V_{LW} and the right ventricular free wall V_{RW}. A schematic representation of the model is presented in Figure 4.7. The model enable simulation of the left and right ventricle and the interaction between the two is derived via the interventricular septum. The same way as for the atria, the cavity volumes are state variables varying over time whereas the wall volumes are constant, see Table A.4.

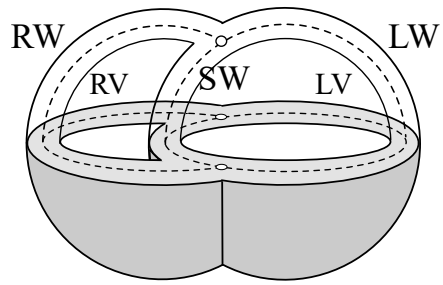

Figure 4.7: Geometrical representation of the ventricular three-wall segment element. The element enclose the left (LV) and right (RV) ventricular blood volume within the left (LW) and right (RW) ventricular free wall and the septal wall (SW). Figure adapted from [21].

Recall that the midwall is defined for any spherical wall segment as the surface that divides the wall volume V_W in an inner and outer shell of equal volume. The midwall volume V_m of a ventricular wall is defined as the volume enclosed by the midwall surface of the corresponding wall and the plane of the junction circle with radius y_m, see Figure 4.8.

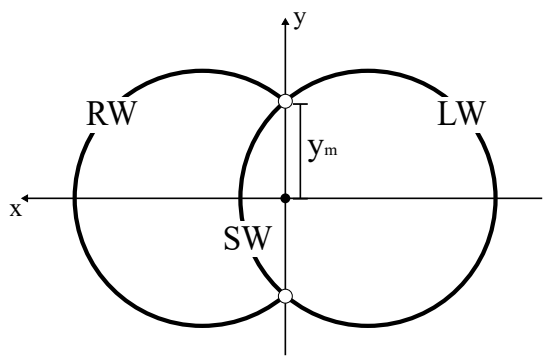

Figure 4.8: A cross-section representation of the three-wall segment model. The midwall surface of each wall are represented as the bold line. A coordinate system is introduced with origo in the black dot so that the y-axis coincide with the sphere-sphere intersection and the x-axis gives rotational symmetry around its axis. y_m is the junction radius of the circle arising due to sphere-sphere intersection.

The septal midwall volume $V_{m,SW}$ and the junction radius y_m are state variables and are known from their preceding time points or their initial values, see Table A.10. Given the septal midwall volume, the left midwall volume $V_{m,LW}$ and the right midwall volume $V_{m,RW}$ can be expressed as,

$$\begin{cases} V_{m,LW} &= -V_{LV} - \frac{1}{2}V_{LW} - \frac{1}{2}V_{SW} + V_{m,SW} \\ V_{m,RW} &= +V_{RV} + \frac{1}{2}V_{RW} + \frac{1}{2}V_{SW} + V_{m,SW}. \end{cases} \tag{4.20}$$

For a more graphical representation of this equation system see Figure 4.9.

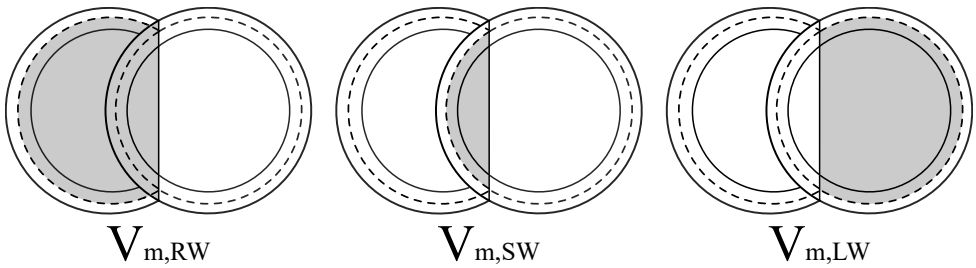

Figure 4.9: Graphical representations of the right midwall volume $V_{m,RW}$ (left panel), septal midwall volume $V_{m,SW}$ (middle panel) and left midwall volume $V_{m,LW}$ (right panel) depicted in grey.

Note that the right midwall volume is defined positive and the left midwall volume is defined negative. This is a result of the definition of a positive midwall volume V_m if the current wall curvature is convex to the positive x-axis, see the coordinate system of Figure 4.8. This will be motivated by further calculations.

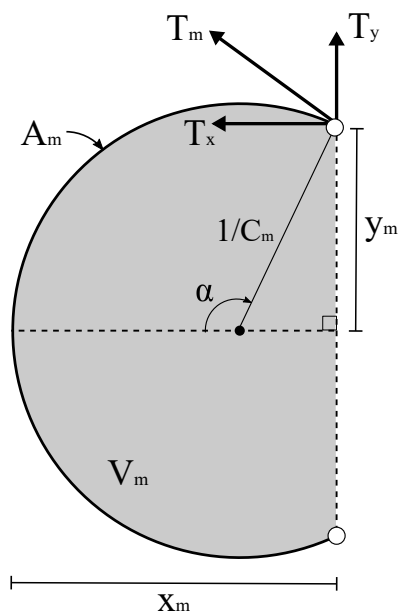

Figure 4.10: Cross-section representation of the midwall geometry of a single wall of the three-wall segment. Each wall have a midwall surface area A_m and a midwall volume V_m (depicted in grey). A two dimensional coordinate system give the tension T_m of each wall as a resultant of the tension along the x-axis T_x and the y-axis T_y. Figure adapted from [21].

Introducing the geometry given in Figure 4.10, it follows from the volume of a spherical cap that,

$$V_m = \frac{\pi}{6} x_m (x_m^2 + 3y_m^2) \tag{4.21}$$

which can be rewritten with x_m as the unknown variable as,

$$x_m = \begin{cases} Q - \dfrac{y_m^2}{Q} & \text{for RW and SW} \\ \dfrac{y_m^2}{Q} - Q & \text{for LW} \end{cases} \tag{4.22}$$

with,

$$Q = \left(\sqrt{\left(\frac{3V_m}{\pi}\right)^2 + y_m^6} + \frac{3|V_m|}{\pi} \right)^{1/3}. \tag{4.23}$$

The relations for the midwall surface area A_m and the curvature C_m can be expressed from x_m and y_m as,

$$A_m = \pi(x_m^2 + y_m^2) \tag{4.24}$$

$$C_m = \frac{2x_m}{x_m^2 + y_m^2} \tag{4.25}$$

due to geometry. The same way as for the atrium, the resultant tension T_m in each wall can be calculated as,

$$T_m = \frac{dT}{dA}(A_m - A_{m0}) \tag{4.26}$$

where dT/dA is the wall area stiffness varying over time and A_{m0} is the midwall area at zero tension. The tension of each wall is used later on to model sarcomere contraction.

Since the tension T_m of each ventricular wall is a function of the three-wall segment geometry, the septal midwall volume $V_{m,SW}$ and junction radius y_m can be adjusted numerically using Newtons method. Using trigonometry of Figure 4.10 it can be proven, see Appendix B.2, that the tension components of T_m in the x-direction T_x and the y-direction T_y can be expressed as,

$$\begin{cases} T_x = T_m \cdot \sin(\alpha) & \text{with } \sin(\alpha) = \dfrac{2x_m y_m}{x_m^2 + y_m^2} \\ T_y = T_m \cdot \cos(\alpha) & \text{with } \cos(\alpha) = \dfrac{-x_m^2 + y_m^2}{x_m^2 + y_m^2} \end{cases} \tag{4.27}$$

for all three walls. Using these components, the resultant tensions of the full three-wall segment in the x-direction, $T_{x,TriSeg}$, and the y-direction, $T_{y,TriSeg}$, can be calculated as,

$$T_{x,TriSeg} = \frac{T_{x,LW} + T_{x,SW} + T_{x,RW}}{\sqrt{T_{m,LW}^2 + T_{m,SW}^2 + T_{m,RW}^2}} \tag{4.28}$$

$$T_{y,TriSeg} = \frac{T_{y,LW} + T_{y,SW} + T_{y,RW}}{\sqrt{T_{m,LW}^2 + T_{m,SW}^2 + T_{m,RW}^2}}. \tag{4.29}$$

The new estimations of the septal midwall volume and junction radius for each time step are then given by linearization and Newtons method as,

$$\begin{cases} V_{m,SW}^{(k+1)} & = V_{m,SW}^{(k)} - dV \\ y_m^{(k+1)} & = y_m^{(k)} - dY \end{cases} \tag{4.30}$$

with,

$$\begin{cases} dV & = \dfrac{1}{\det(\mathbf{J}_T)} \Big(\dfrac{dT_{y,TriSeg}}{dy} T_{x,TriSeg}^{(k)} - \dfrac{dT_{x,TriSeg}}{dy} T_{y,TriSeg}^{(k)} \Big) \\ dY & = \dfrac{1}{\det(\mathbf{J}_T)} \Big(- \dfrac{dT_{y,TriSeg}}{dv} T_{x,TriSeg}^{(k)} + \dfrac{dT_{x,TriSeg}}{dv} T_{y,TriSeg}^{(k)} \Big). \end{cases} \tag{4.31}$$

Here $\mathbf{J}_T$ is the Jacobian matrix of the three-wall segment tension. For the proof of this see Appendix B.3. The state variable derivatives $\dot{V}_{m,SW}$ and $\dot{y}_m$ are calculated as,

$$\begin{cases} \dot{V}_{m,SW} & = \dfrac{dV}{\tau} \\ \dot{y}_m & = \dfrac{dY}{\tau} \end{cases} \tag{4.32}$$

using Equation (4.31) for $k = 1$ with τ being a time scaling parameter presented in Table A.4. Using Equation (4.30) repeatedly a new estimation $k + 1$ can be made from previous estimation k and the tension components of the full three-wall segment. The first estimation $k = 1$ is set from previous time step and the process is executed until the estimations converges. The new converged values are then used as the true state variable values.

Using the converged estimations of $V_{m,SW}$ and y_m, Equation (4.20)-(4.26) can be executed again for the new geometry. The equation for the transmural pressure p_W derived for the spherical atrium,

$$p_W = 2T_m C_m \tag{4.33}$$

also holds for spherical segments and therefore holds for the walls of the ventricular segment [21]. The transmural pressure of the left and right ventricular free wall will be used later on to determine cavity pressure.

Lastly the cross-section area of the left A_{LV} and right A_{RV} ventricles are given by,

$$\begin{cases} A_{LV} & = \dfrac{V_{LV} + 0.55V_{LW} + 0.55V_{SW}}{2(V_{LV} + V_{LW} + V_{SW})^{1/3}} \\ A_{RV} & = \dfrac{V_{RV} + 0.55V_{RW} + 0.55V_{SW}}{2(V_{RV} + V_{RW} + V_{SW})^{1/3}} \end{cases} \tag{4.34}$$

and the wave impedance Z is calculated as,

$$\begin{cases} Z_{LV} &= \dfrac{0.2\sqrt{2\rho(V_{LV}+V_{LW}+V_{SW})^{1/3}\left|\dfrac{dT}{dA}\right|}}{A_{LV}} \\ Z_{RV} &= \dfrac{0.2\sqrt{2\rho(V_{RV}+V_{RW}+V_{SW})^{1/3}\left|\dfrac{dT}{dA}\right|}}{A_{RV}}. \end{cases} \tag{4.35}$$

Similar to the atria, the wave impedance is used as a measurement of resistance in the cavities and will be used to determine blood flow.

4.4.4 Sarcomere mechanics model

Cardiac pumping in atria and ventricles during a cardiac cycle is modeled using sarcomere mechanics within the myocardial walls. Each myocardial wall is divided into patches and the sarcomere mechanics is modeled for each patch separately. For the original CircAdapt model there is a total of five patches, one for each wall. The methodology of the sarcomere mechanics model is presented in the appendix of the ventricular three-wall segment model article by Lumens et al. [21], in the multipatch article by Walmsley et al. [22] and in the latter articles data supplement. For each patch the sarcomere mechanics model calculate the stress σ of a patch as a function of the strain ε and other model parameters. The parameter values of the sarcomere mechanics model parameters are presented in Table A.5 of Appendix A.1.

The stress σ of each patch of cardiac muscle is divided into two terms, an active σ_{act} and a passive σ_{pas} term,

$$\sigma = \sigma_{act} + \sigma_{pas} \tag{4.36}$$

which gives the following differential equation of the stress as a function of the strain,

$$\frac{d\sigma}{d\varepsilon} = \frac{d\sigma_{act}}{d\varepsilon} + \frac{d\sigma_{pas}}{d\varepsilon}. \tag{4.37}$$

The active stress occur due to muscle fiber contraction and the passive stress arises from soft tissue deformation of the myocardium.

The active stress depends on two variables, the intrinsic sarcomere length L_{si} and the contractility C. The contractility is introduced to model cross-bridge formation density between thick and thin filaments of each patch. Recall from Table 4.2 that both the intrinsic sarcomere length and the contractility are state variables of the ordinary differential equation solver. The differential equation determining the intrinsic sarcomere length is,

$$\dot{L_{si}} = v_{max}\left(\frac{L_s - L_{si}}{L_{se,iso}} - 1\right) \tag{4.38}$$

with $\dot{L_{si}}$ being the state variable time derivative. $L_{se,iso}$ is the length of the series elastic element during isovolumetric contraction, v_{max} is velocity of sarcomere shortening at zero load and,

$$L_s = L_{sRef} \cdot e^{\varepsilon} \tag{4.39}$$

is the total sarcomere length with L_{sRef} being a parameter of reference sarcomere length.

The differential equation determining the contractility state variable C is given by,

$$\dot{C} = \frac{1}{t_{rise}} F(L_{si}) \cdot R(t) - \frac{1}{t_{decay}} C \cdot G(X). \tag{4.40}$$

with $\dot{C}$ being the state variable time derivative. The time parameters,

$$t_{rise} = 0.55 T_R t_{a/v} \tag{4.41}$$

$$t_{decay} = 0.33 T_D t_{a/v} \tag{4.42}$$

are the rise time and the decay time parameters determined by the time parameters T_R and T_D. $t_{a/v}$ is the duration of the myocardial activation determined for atrial and ventricular patches in Equation (4.7) and (4.8) respectively. The first term function $F(L_{si})$ describes the cross-bridge formation between the thick and thin filaments as a function of intrinsic sarcomere length,

$$F(L_{si}) = \tan^{-1}\left(0.75 \cdot 9.1204 \cdot L^2\right) \tag{4.43}$$

where,

$$L = \frac{L_{si}}{L_{si0}} - 1 \tag{4.44}$$

and L_{si0} is the sarcomere length of no active stress. The function $R(t)$ model the rate of cross-bridge formation as,

$$R(t) = 0.02 x^3 (8 - x)^2 e^{-x} \tag{4.45}$$

for,

$$x(t) = \min\left(8, \max(0, \frac{t_c}{t_{rise}})\right). \tag{4.46}$$

Here t_c is a time variable calculated as a function of the current time t, the cardiac cycle time parameter t_{CC} and the time parameter of wall activation determined for each wall patch in Equation (4.1)-(4.5). The second term equation $G(X)$ represents an exponential decay in contractility by,

$$G(X) = 0.5 + 0.5 \cdot \sin\left(\text{sign}(X) \cdot \min(\frac{\pi}{2}, |X|)\right) \tag{4.47}$$

for,

$$X = \frac{t_c - t_A}{t_{decay}} \tag{4.48}$$

$$t_A = 0.65 + 1.0570 t_{a/v} L. \tag{4.49}$$

Knowing the differential equation describing the contractility C and the intrinsic sarcomere length L_{si} the active stress σ_{act} can be calculated as,

$$\sigma_{act} = 1.51 \sigma_{f,act} L \Big(C \frac{L_s - L_{si}}{L_{se,iso}} \Big) \tag{4.50}$$

with $\sigma_{f,act}$ being an active stress parameter. Recalling the relation between sarcomere length L_s and strain ε given in Equation (4.39) the derivative of the active stress as a function of the strain can be expressed as,

$$\frac{d\sigma_{act}}{d\varepsilon} = 1.51 \sigma_{f,act} L C \frac{L_{sRef}}{L_{se,iso}} e^{\varepsilon}. \tag{4.51}$$

The passive stress σ_{pas}, occurring due to myocardial soft tissue deformation, can be split into two terms. The first term σ_{ECM} contains the stress arising from the extracellular matrix surrounding the muscle cells. The second term σ_{int} is the stress that the internal structures of the muscle cells and sarcomeres create upon themselves,

$$\sigma_{pas} = \sigma_{ECM} + \sigma_{int}. \tag{4.52}$$

The stress arising from the extracellular matrix is given by,

$$\sigma_{ECM} = 0.0349 \sigma_{f,pas} (\lambda_{s,pas}^{10} - 1) \tag{4.53}$$

where

$$\lambda_{s,pas} = \frac{L_{sRef}}{L_{s0,pas}} \cdot e^{\varepsilon} \tag{4.54}$$

with $L_{s0,pas}$ a different reference sarcomere length for passive stress and $\sigma_{f,pas}$ is a passive stress parameter. The internal structure is not as stiff as the extracellular matrix and is proportional to the active stress stiffness as,

$$\sigma_{int} = 0.01 \sigma_{f,act} (\lambda_{s,pas}^{k} - 1) \tag{4.55}$$

with,

$$k = 2 \frac{L_{sRef}}{dL_{s0,pas}} \tag{4.56}$$

and $dL_{s0,pas}$ a passive stress sarcomere length parameter. Using the calculated stresses, the passive stress derivative as a function of the strain can be expressed as,

$$\frac{d\sigma_{pas}}{d\varepsilon} = 0.349\sigma_{f,pas}\lambda_{s,pas}^{10} + 0.01k\sigma_{f,act}\lambda_{s,pas}^{k}. \quad (4.57)$$

The total stress σ and stress derivative $d\sigma/d\varepsilon$ of a sarcomere, and a wall patch, can be calculated from the active and passive components using Equation (4.36) and (4.37). The components are used to calculate the wall tension and wall area stiffness of the myocardial wall patches.

4.4.5 Myocardial patch model

The sarcomere mechanics presented in previous subsection describes the mechanical events within one patch, see Figure 4.11. The myocardial patch model is used to connect the sarcomere mechanics within each patch to the mechanics of the full wall, as well as modeling the tension and surface area properties of myocardial contraction. The theory of the myocardial patch model is presented in the MultiPatch article by Walmsley et al. [22] and the execution of this is presented in the source code [18]. The parameters used within the myocardial patch model are presented in Table A.6.

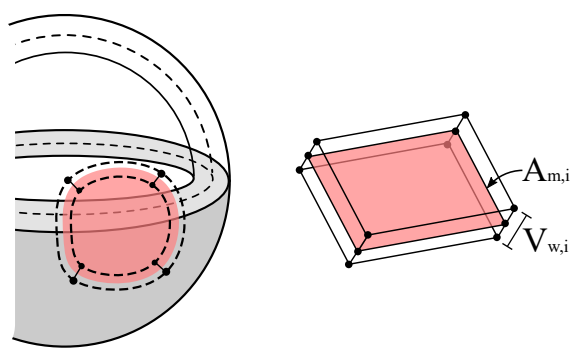

Figure 4.11: The patch model of the myocardial wall. Each wall is subdivided into a number of patches j, in this case one. Each patch i has a midwall area $A_{m,i}$ and a wall volume $V_{W,i}$. Figure adapted from [22].

The strain ε and midwall surface area $A_{m,i}$ of the i:th patch of each wall depend on the intrinsic sarcomere length L_{si} as,

$$\varepsilon = \ln\left(\frac{L_{si}}{L_{sRef}}\right) \quad (4.58)$$

$$A_{m,i} = A_{mRef}\left(\frac{L_{si}}{L_{sRef}}\right)^2 \quad (4.59)$$

where A_{mRef} is the reference midwall area at reference sarcomere length L_{sRef}. Further the strain and the corresponding stress σ, according to sarcomere mechanics, give rise to a patch tension $T_{m,i}$ and a wall area stiffness $(dT/dA)_i$ as,

$$T_{m,i} = \frac{\sigma V_{W,i}}{2A_{m,i}} \tag{4.60}$$

$$\left(\frac{dT}{dA}\right)_i = \left(\frac{d\sigma}{d\varepsilon} - 2\sigma\right)\frac{V_{W,i}}{4A_{m,i}^2} \tag{4.61}$$

where $V_{W,i}$ is the wall volume of the corresponding i:th patch of the wall. Rearranging the tension equation of a full wall presented for atria and ventricles in Equation (4.16) and (4.26), the patch midwall area at zero tension $A_{m0,i}$ can be calculated as,

$$A_{m0,i} = A_{m,i} - \frac{T_{m,i}}{(dT/dA)_i}. \tag{4.62}$$

Previous calculations of wall dimensions and material properties can be transferred between a patch and a wall using linearity. For each patch i it holds that the tension $T_{m,i}$ is equal to the tension of the full wall T_m,

$$T_{m,i} = T_m \tag{4.63}$$

and for each wall with j patches it holds that,

$$V_W = \sum_{i=1}^{j} V_{W,i} \tag{4.64}$$

$$A_{m0} = A_{mDead} + \sum_{i=1}^{j} A_{m0,i} \tag{4.65}$$

$$\frac{dT}{dA} = \frac{1}{\sum_{i=1}^{j}\left(\frac{dT}{dA}\right)_i^{-1}}. \tag{4.66}$$

The parameter A_{mDead} is the non-contractile area of the full wall, see Table A.7. Since the original CircAdapt model is based on only one patch per wall, i.e. $j = 1$, Equation (4.65) is the only equation where the calculated variable differ between the wall and its patch, due to the non-contractile area term.

Recall from the flow chart in Figure 4.3 that the myocardial patch model is called twice for each time step. This connects the calculations executed on the full wall, within the atrial chamber model and the ventricular three-wall segment model, to the calculations executed on each patch, within the sarcomere mechanics model.

4.4.6 Pericardium model

The pericardium model models the pericardium as a passive elastic bag enclosing all four cavities of the heart and their corresponding walls. The pericardium is assumed to not have any cavity of its own and to be a very thin wall of zero volume. The pericardium model is described in the CircAdapt Simulator manual [16] and in the MATLAB source code [18].

The model calculate the pericardium enclosed volume, i.e. the total heart volume, V_p as,

$$V_p = \sum_n V_n + \sum_m V_m \tag{4.67}$$

where $n = [LA\ RA\ LV\ RV]$ and $m = [LAW\ RAW\ LW\ SW\ RW]$, i.e. the sum of the cavity volumes and wall volumes of the heart components.

The transmural pressure p_W of the pericardium can be expressed as a function of the enclosed volume as,

$$p_W = p_{ref}\left(\frac{V_p}{V_{ref}}\right)^k \tag{4.68}$$

where p_{ref} is the reference pressure at the reference volume V_{ref} and k is the stiffness exponent of the pericardium. The parameter values of the pericardium model are presented in Table A.8. The pericardium transmural pressure is used later on to calculate cavity pressure within the heart.

4.4.7 Cavity pressure model

The cavity pressure model calculates cavity pressure of all cavities included in the model, i.e. blood vessels and heart cavities. The execution of the model is described in the CircAdapt source code [18] and uses the concept of transmural pressure. The general definition of transmural pressure p_W is,

$$p_W = p_{in} - p_{out} \tag{4.69}$$

where p_{in} and p_{out} are the cavity pressures of the inner and outer structure respectively [1].

The pericardium is assumed to not be enclosed by any outer wall. Therefore the pressure within the pericardium p_p is equal to the transmural pressure p_W of the pericardium wall calculated in Equation (4.68),

$$p_p = p_W. \tag{4.70}$$

The definition of transmural pressure and the pericardium pressure give the atrial cavity pressure as,

$$\begin{cases} p_{LA} &= p_p + p_{W,LAW} \\ p_{RA} &= p_p + p_{W,RAW} \end{cases} \tag{4.71}$$

where $p_{W,LAW}$ and $p_{W,RAW}$ are the transmural pressures of the atrial walls calculated in Equation (4.17). Similarly, the pressure of the ventricular cavities are calculated as,

$$\begin{cases} p_{LV} &= p_p - p_{W,LW} \\ p_{RV} &= p_p + p_{W,RW}. \end{cases} \tag{4.72}$$

where the ventricular free wall transmural pressures $p_{W,LW}$ and $p_{W,RW}$ are calculated in Equation (4.33). The negative sign of the left ventricular expression occur due to the defined x-axis of the three-wall segment model, which gives a negative curvature C_m of the left ventricular free wall and thus a negative transmural pressure.

The arteries and veins are assumed to be enclosed only by the arterial and venous wall and no additional outer boundary. This result in a pressure calculation of the arterial and venous pressures, similar to the pressure of the pericardium, depending only on the own wall,

$$\begin{cases} p_{SyArt} &= p_{W,SyArt} \\ p_{SyVen} &= p_{W,SyVen} \\ p_{PuArt} &= p_{W,PuArt} \\ p_{Puven} &= p_{W,PuVen}. \end{cases} \tag{4.73}$$

The transmural wall pressures, i.e. the right side of Equation (4.73), are calculated in Equation (4.9) for each vessel.

4.4.8 Cavity flow model

The cavity flow model connects the blood vessel model, the atrial chamber model and the ventricular three-wall segment model into a closed loop model of the blood circulation. The model creates the closed loop by connecting adjacent cavities using valves, capillary networks and inflow channels and determine blood flow through the cavities. The execution of the model is presented in the MATLAB source code [18].

To connect all components into a closed-loop model of the cardiovascular system, nodes are placed within each cavity, see Figure 4.12. The four chambers of the heart are adjacent to three different valves whereas the four blood vessels of the two circulations are adjacent to one or two valves and one capillary network. Note that the right and left atrial inflow, ASD, VSD and PDA are modeled as valves, even though this is not physiologically correct.

The blood flow through a cavity node q_N is defined as the inflow q_{in} minus the outflow q_{out},

$$q_N = \sum q_{in} - \sum q_{out}. \tag{4.74}$$

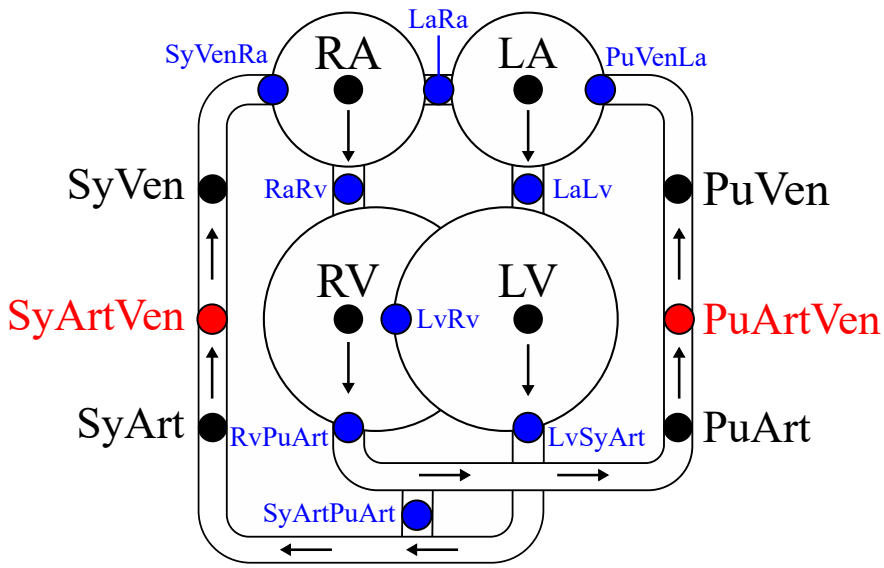

Figure 4.12: A schematic presentation of the model representation of nodes (black dots), capillary networks (red dots) and valves (blue dots). The arrows show the direction of the circulation.

The flow through the nodes is therefore a combination of a minimum of two terms, each representing either flow through a valve or flow through a capillary network. Recall that the valve flow of all nine valves are known state variables, see Table 4.2. The flow through the nodes of the four heart chambers all depend on the flow through different valves as,

$$q_{N,LA} = q_{PuVenLa} - q_{LaLv} - q_{LaRa} \tag{4.75}$$
$$q_{N,RA} = q_{SyVenRa} - q_{RaRv} + q_{LaRa} \tag{4.76}$$
$$q_{N,LV} = q_{LaLv} - q_{LvSyArt} - q_{LvRv} \tag{4.77}$$
$$q_{N,RV} = q_{RaRv} - q_{RvPuArt} + q_{LvRv}. \tag{4.78}$$

The flow through the nodes of the systemic and pulmonary arteries and veins all depend on one or two terms of flow through a valve and one term of flow through the pulmonary capillary network $q_{PuArtVen}$ or the systemic capillary network $q_{SyArtVen}$ as follows,

$$q_{N,SyArt} = q_{LvSyArt} - q_{SyArtVen} - q_{SyArtPuArt} \tag{4.79}$$
$$q_{N,SyVen} = q_{SyArtVen} - q_{SyVenRa} \tag{4.80}$$
$$q_{N,PuArt} = q_{RvPuArt} - q_{PuArtVen} + q_{SyArtPuArt} \tag{4.81}$$
$$q_{N,PuVen} = q_{PuArtVen} - q_{PuVenLa}. \tag{4.82}$$

The flow through both capillary networks depend on a pressure drop occurring when the blood flows through the capillaries. This capillary flow q_{ArtVen} is determined

by,

$$q_{ArtVen} = q_{Ref,ArtVen}\left(\frac{p_{Art} - p_{Ven}}{p_{Ref,ArtVen}}\right)^{k_{ArtVen}} \tag{4.83}$$

where p_{Art} and p_{Ven} are the cavity pressures of the artery and vein of the corresponding circulation. k_{ArtVen} is the stiffness exponent parameter and $q_{Ref,ArtVen}$ is the reference flow at the reference pressure drop $p_{Ref,ArtVen}$. The values of the capillary network parameters for the systemic network and the pulmonary network are presented in Table A.2. The reference pressure drop of the systemic capillary network is the only parameter that changes throughout the simulation. After each completed cardiac cycle, this parameter value is adapted to match the cardiac output q_0, mean arterial pressure p_0 and the systemic vessel pressure-flow relation throughout the simulated heart beat.

Using the nodal flow q_N for each node, the derivative of the cavity volume, i.e. the cavity blood flow, can be calculated. The total flow $q_{N,tot}$ through a node can be calculated as a summation of the previously calculated nodal flow q_N, that is an effect of hemodynamics, and the cavity flow that is an effect of physical properties,

$$q_{N,tot} = q_N + \frac{p}{Z}. \tag{4.84}$$

The second term is the flow of the cavity using Ohms law applied on the cavity pressure p calculated in Section 4.4.7 and the resistance, given by the wave impedance Z, calculated in Equation (4.11) for the blood vessels and Equation (4.19) and (4.35) for the heart cavities. The nodal pressure p_N is given by,

$$p_N = q_{N,tot} \cdot Z \tag{4.85}$$

which is used later on, together with the nodal flow, to calculate the valve flow derivatives. Lastly the time derivative of the cavity volume $\dot{V}$ is calculated as,

$$\dot{V} = \frac{p_N - p}{Z} \tag{4.86}$$

which is, recalling Table 4.2, the derivative of a state variable.

4.4.9 Valve flow model

The valve flow model uses adjacent cavities to each valve and pressure gradients across the valves to determine the valve flow derivatives of the circulation. The execution of this have been found by studying the MATLAB source code [18].

Every valve is in direct connection to a proximal cavity and a distal cavity, see Figure 4.12. The proximal cavity is defined as the cavity located before the valve and the distal cavity defined as being located after the valve in the direction of the blood circulation. The definition of a proximal and distal cavity result in defining

the direction of valve flow q, which is a state variable. A positive flow is defined as blood flow from the proximal cavity to the distal cavity. A negative flow is defined as blood flow from the distal cavity to the proximal cavity. The pressure gradient dp between the two cavity nodes can be calculated as the difference in proximal cavity node pressure $p_{N,prox}$ and distal cavity node pressure $p_{N,dist}$,

$$dp = p_{N,prox} - p_{N,dist}. \tag{4.87}$$

The node pressures are calculated in Equation (4.85).

The model defines three states of each valve based on pressure and physiological knowledge of how the valves operate;

$$\begin{cases} dp > 0 & \longrightarrow \text{The valve is } \textit{open} \\ dp < 0 \begin{cases} \text{and } q > 0 & \longrightarrow \text{The valve is } \textit{closing} \\ \text{and } q < 0 & \longrightarrow \text{The valve is } \textit{closed}. \end{cases} \end{cases} \tag{4.88}$$

The flow derivatives during these three cases can be determined by calculating the Bernoulli pressure drop according to hemodynamics as presented by Westerhof et al [15]. The Bernoulli pressure drop is for all three cases proportional to the cross-section area susceptible to blood flow, see Figure 4.13.

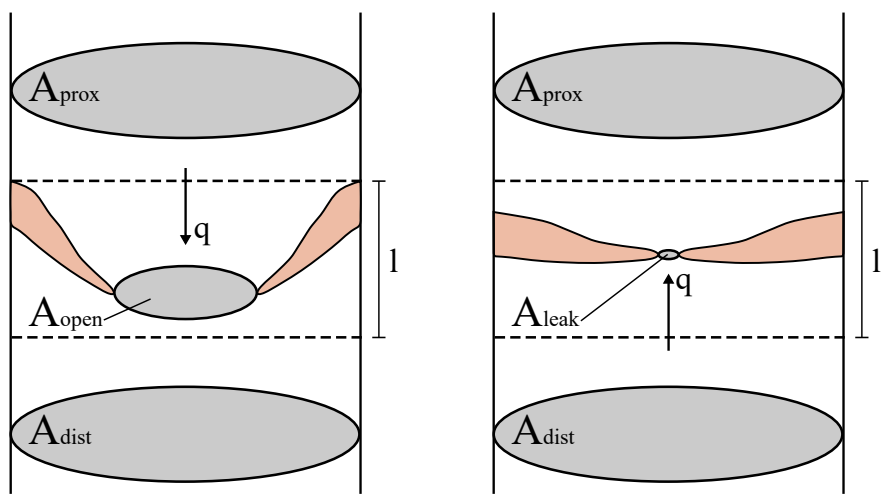

Figure 4.13: Graphical representation of the geometry determining blood flow through the valves. The figure show cross-section areas of the proximal A_{prox} and distal A_{dist} cavity, valve dimensions and flow direction for an open/closing valve (left panel) and closed valve (right panel).

The susceptible area during forward flow A_{fw} and backward flow A_{bw} are determined as,

$$A_{fw} = \min(A_{prox}, A_{dist}, A_{open}) \tag{4.89}$$
$$A_{bw} = \min(A_{prox}, A_{dist}, A_{leak}) \tag{4.90}$$

where A_{prox} and A_{dist} are the cross-section areas of the proximal and distal cavities respectively, calculated for the blood vessels in Equation (4.10) and for heart cavities in Equation (4.18) and (4.34). A_{open} and A_{leak} are the cross-section area of an open and closed valve respectively and are parameters specific for each valve, see Table A.9 of Appendix A.1. To include the papillary muscles within the ventricles in the model, the parameter A_{leak} of the mitral valve (LaLv) and the tricuspid valve (RaRv) are determined as variables as,

$$A_{leak} = 0.1A_{open} \cdot \tanh\Big(100 \cdot \max\big(0.001, \frac{T_m}{\frac{dT}{dA}A_{m0}} - 0.1\big)^2\Big) \quad (4.91)$$

where T_m, A_{m0} and dT/dA are the tension, zero tension midwall surface area and wall area stiffness of the left and right ventricular free wall. The Bernoulli pressure drop dp_B of the three valve states can then be calculated as a function of forward flow orifice area A_{fw} or backward flow orifice area A_{bw} as,

$$dp_B = \begin{cases} \frac{1}{2}\rho q^2\Big(\frac{1}{A_{fw}^2} - \frac{1}{A_{prox}^2}\Big) & \text{if the valve is } \textit{open} \\ \frac{1}{2}\rho q^2\Big(\frac{1}{A_{closing}^2} - \frac{1}{A_{prox}^2}\Big) & \text{if the valve is } \textit{closing} \\ -\frac{1}{2}\rho q^2\Big(\frac{1}{A_{bw}^2} - \frac{1}{A_{dist}^2}\Big) & \text{if the valve is } \textit{closed}. \end{cases} \quad (4.92)$$

The cross-section area of a closing valve $A_{closing}$ is given by,

$$A_{closing} = \sqrt{\frac{x}{\sqrt{x^2+y^2+400}}} \cdot \big(A_{fw} - A_{bw}\big) + A_{bw} \quad (4.93)$$

where,

$$x = \frac{40 \cdot \rho q \cdot |q|}{A_{fw}^2} \quad (4.94)$$

$$y = dp. \quad (4.95)$$

Lastly, the state variable valve flow derivatives $\dot{q}$ are calculated as,

$$\dot{q} = \begin{cases} \dfrac{dp_B - dp}{\frac{3}{2}\rho\Big(\frac{l}{A_{fw}} + \frac{1}{2}\Big(\frac{1}{\sqrt{A_{prox}}} + \frac{1}{\sqrt{A_{dist}}}\Big)\Big)} & \text{if the valve is } \textit{open} \\ \dfrac{dp_B - dp}{\frac{3}{2}\rho\Big(\frac{l}{A_{closing}} + \frac{1}{2}\Big(\frac{1}{\sqrt{A_{prox}}} + \frac{1}{\sqrt{A_{dist}}}\Big)\Big)} & \text{if the valve is } \textit{closing} \\ \dfrac{dp_B - dp}{\frac{3}{2}\rho\Big(\frac{l}{A_{bw}} + \frac{1}{2}\Big(\frac{1}{\sqrt{A_{prox}}} + \frac{1}{\sqrt{A_{dist}}}\Big)\Big)} & \text{if the valve is } \textit{closed} \end{cases} \quad (4.96)$$

where l is the length of the valve, see Table A.9.

Recall that ASD, VSD and PDA are modeled as valves. The default blood flow direction can be seen in Equation (4.75)-(4.78), (4.79) and (4.81). The model originally models septal defects as blood flow from the left to the right side of the heart and PDA from the systemic artery to the pulmonary artery. However, the model is constructed to handle the opposite direction of flow, simply by changing the parameter values so that $A_{open} < A_{leak}$. However, this change in parameters should not be performed on the true valves or the atrial inflows in order to maintain the physiologically correct direction of circulation.

4.5 Simulation result

The result of the simulation, both parameters used and the simulated dynamics over time, is saved in a structure available to the user once the execution is completed. The result for set number of heart beats is displayed automatically as a single plot. The plot presents cavity pressure, cavity volume and valve flow over time. It also presents pressure as a function of volume in the heart cavities and stress as a function of strain in the myocardial walls. Here, the input parameters mean aortic pressure p_0 and cardiac output q_0, see Table 4.1, are used to scale the resulting dynamical properties to match the input amplitude of pressure and flow.

A user constructed Wigger diagram of the result of the original CircAdapt model simulation is presented in Figure 4.14.

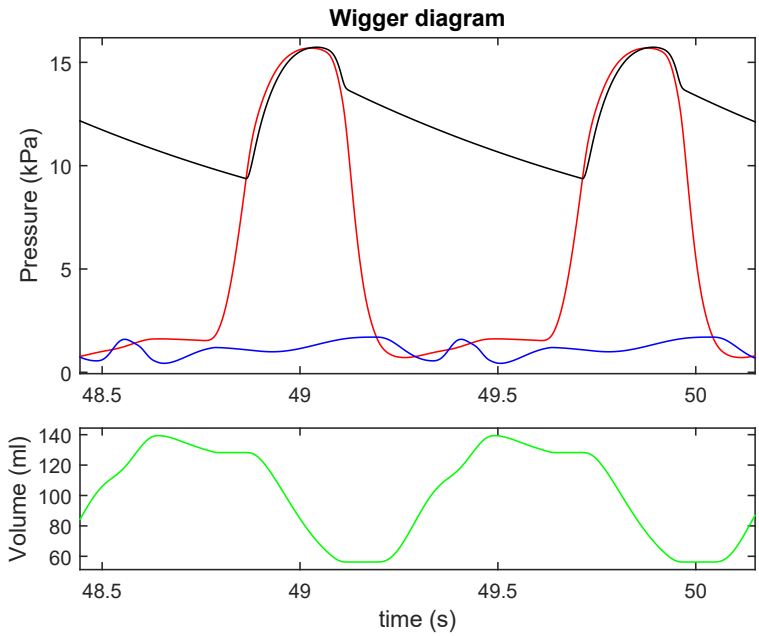

Figure 4.14: Wigger diagram constructed of the last two heartbeats of the original CircAdapt model with default heart cycle time $t_{CC} = 0.85$s and a total simulation time of 50 seconds, i.e. $N_{HB} = 59$ heartbeats. The mean aortic pressure p_0 and cardiac output q_0 are set to default value. No scaling for mean aortic pressure p_0 or cardiac output q_0 is executed. The upper plot show pressure of the left ventricle (red line), aorta (black line) and left atrium (blue line). The lower plot show the left ventricular volume (green line).

4.6 Model limitations

The CircAdapt simulation model is a mathematical model and therefore have limitations in simulating a complex biological system that depend on human anatomy and physiology. A fundamental and inevitable limitation is the parameters and the mathematical formulas. The parameters used are occasionally difficult to determine for a true cardiovascular system, resulting in parameters that are estimated and might lack physiological relevance. The mathematical equations used are chosen to, as accurately as possible, simulate true physiological behaviour which is often a balance between accuracy and model complexity.

A limitation of the model is that it is constrained to the cardiovascular system, excluding other human body components that have an impact on cardiovascular function, such as other organs, the endocrine system and the nervous system. Another limitation is the relation between two succeeding heart beats, as a new heart beat only depend on the state variable values of the final time step of the previous cardiac cycle. A physiological inaccuracy of the model is the determination of contraction and relaxation of the cardiac muscle as a linear function of the cardiac cycle

time. Chung et al. [23] have shown a non-linear correlation between the duration of diastole, i.e. ventricular relaxation, and the heart rate.

There are several limitations to the functions of the ordinary differential equation solver, constituting the system of differential equations modeling the cardiovascular system. The model include only four blood vessels, which are all modeled as the large vessels leaving and entering the heart. The true large vessels of the cardiovascular system (aorta, vena cava, pulmonary artery and pulmonary vein) do in fact connect to the heart, but are branched into smaller arteries and veins after which the smaller arteries transcend into smaller veins via the capillaries [1]. It can be seen that the model, since it models the cardiovascular system as separate modules, lack some accuracy in modeling local influences of certain events during the cardiac cycle. For example the closing of the aortic valve occur due to backward blood flow pushing the valve closed, which result in an increase in aortic pressure. This increase can be seen in the true Wigger diagram, see Figure 2.10, but not in the Wigger diagram constructed from the result of the CircAdapt model, see Figure 4.14. Another limitation of the valve flow model is the model setup of modeling atrial inflow as valves.

The myocardial patch model and the sarcomere mechanics model are simplified from true myocardial anatomy. The model assumes one single behaviour of the entire myocardial wall, which exclude local differences in myocardial composition. This limitation is extended as the model calculate the stress and strain of the wall as a function of one set of sarcomeres of equal properties. This is a significant simplification, as studies have shown that the cardiac muscle fibers of the ventricle are constructed in a pattern of gradual rotation, when analyzing the myocardium from its outer boundary towards the pericardium to its inner boundary towards the blood [10, 14]. Differences in the rotation of muscle fibers have also been shown along the wall from apex to the AV-plane [10].

4.6.1 Atrial and ventricular model representation

The model representation of atria and ventricles introduces several limitations to the heart anatomy and physiology. The anatomical representation of the atria as two spheres is not geometrically true, as the left and right atrium are joint together with a thin myocardial wall separating the two cavities. The anatomical representation of the ventricles is limited as well as the ventricle is known to more closely resemble an ellipsoid.

Other than the pure geometrical limitation of the heart, spherical segments result in inaccuracies in the model execution of the mechanism of cardiac pumping. Spheres and spherical segments result in a purely radial contraction and relaxation towards the center of the sphere. As have been presented in Section 2.1.6, this is not accurate to the human heart, as radial pumping is only a small portion of the hearts pump function. A measurement of this model limitation can be seen in Figure 4.15,

presenting the total heart volume, normalized to the end diastolic volume. From the data, presented in the figure, the total heart volume variation is collected from the first cycle as 20.4%. Compared to the true value of approximately 8% [10], this is an error that affects the models ability of modeling heart pumping efficiency and the true pumping physiology of the heart.

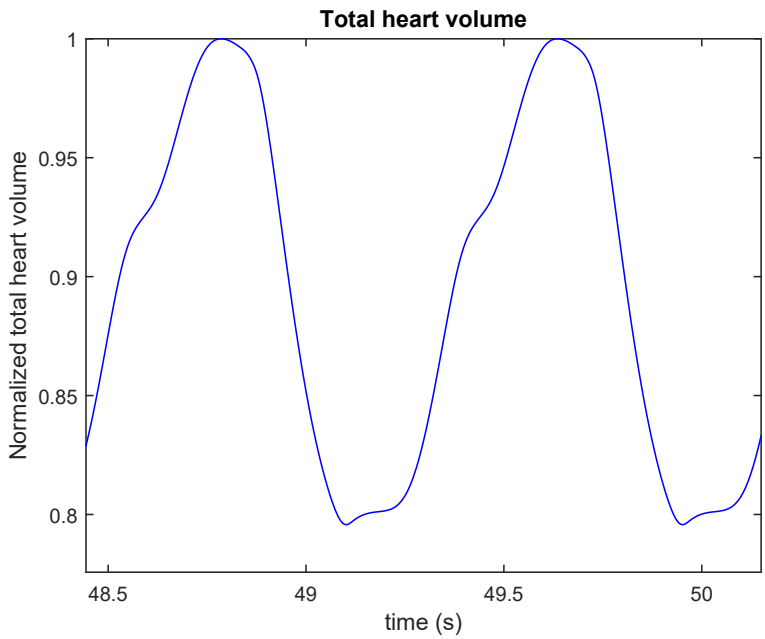

Figure 4.15: Total heart volume of the original CircAdapt model of the last two heartbeats of a simulation with default cardiac cycle time $t_{CC} = 0.85$ s and a total simulation time of 50 seconds, i.e. $N_{HB} = 59$ heartbeats. The total heart volume of the model include the volume of all five myocardial walls and all four heart cavities. The curve is normalized to the end diastolic volume.

Chapter 5

Methods

The method section of this thesis present changes executed on the original CircAdapt model. The focus of these changes are to make the simulation more accurate from a physiological perspective. The adaptations of the CircAdapt model will be executed on the modules representing the heart. Both atria and ventricles are represented as spheres or spherical segments, an approximation that differ from the true heart anatomy. This geometrical representation also result in a simulation based only on radial myocardial contraction, something that has shown to be inaccurate when studying the physiology of cardiac pumping and the resulting total heart volume variation throughout the cardiac cycle [10]. Several different adaptations to the original CircAdapt model will be executed. The aim of each change is to achieve a more accurate geometrical representation of the heart chamber anatomy, as well as improving the model representation of the myocardial contraction by including longitudinal pumping in the model.

5.1 Atrial three-wall segment model

The atrial three-wall segment model is an adaptation of the original CircAdapt model where the atrium is modeled identical to the ventricles. The adaptation consider the atria as a combined segment including two cavities, right (RA) and left (LA) atrium, enclosed and separated by three walls; the left atrial free wall (LAW), the atrial septal wall (SAW) and the right atrial free wall (RAW), see Figure 5.1.

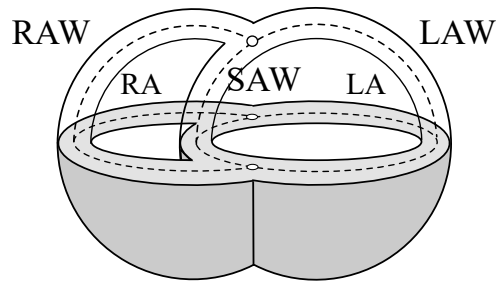

Figure 5.1: The constructed atrial three-wall segment. The model construct the left atrium LA and the right atrium RA enclosed within a left atrial free wall LAW and a right atrial free wall RAW and separated by an atrial septal wall SAW. Figure adapted from [21].

5.1.1 Model parameters and state variables

All myocardial material parameters used to model the sarcomere contraction are unchanged for the left and right atrial wall patch, see Table A.5. The sarcomere mechanics parameters of the introduced septal wall patch are set equal to the left atrial wall patch values, see Table A.5. The remaining parameters changed or included are presented in Table 5.1.

DESCRIPTION	LAW	SAW	RAW
Non-contractile area	$A_{mDead,LAW}$	$A_{mDead,SW}$	$A_{mDead,RAW}$
Patch wall volume	$0.82V_{LAW1}$	$0.18V_{LAW1}$	$0.59V_{RAW1}$
Reference midwall area	$0.83A_{mRef,LAW1}$	$0.18A_{mRef,LAW1}$	$0.91A_{mRef,RAW1}$
Wall volume	$0.82V_{LAW}$	$0.18V_{LAW}$	$0.59V_{RAW}$

Table 5.1: Parameters of the atrial three-wall segment model for the left atrial wall (LAW), septal atrial wall (SAW) and right atrial wall (RAW). The new parameters are expressed as a percentage of the original model parameter, presented in Table A.3, A.6 and A.7 of Appendix A.1.

The number of state variables, see Table 4.2, are increased to include the septal midwall volume and junction radius of the atrial three-wall segment, the atrial septal wall patch contractility and intrinsic sarcomere length. Thus increasing the number of state variables from 30 to 34. All initial values of the right and left atrium are unchanged, see Table A.10. The four new state variable initial values are presented in Table 5.2.

VARIABLE DESCRIPTION	NOTATION	UNIT	VALUE
Contractility	C	SAW1	$9.4085 \cdot 10^{-16}$
Intrinsic sarcomere length	L_{si}	SAW1	2.0218
Midwall volume	V_m	SAW	$6.2775 \cdot 10^{-6}$
Junction radius	y_m	ATriSeg	0.0195

Table 5.2: Adapted state variable initial values of implementing an atrial three-wall segment. The variables are values of the atrial septal wall (SAW), the atrial septal wall patch (SAW1) and the atrial three-wall segment (ATriSeg).

The theory of the calculations of the adapted parameter values and state variable initial values are presented in Appendix C.1.

5.1.2 Implementation

The new representation of the atria result in a few changes in the myocardial activation pattern. The time parameters determining the myocardial activation and contraction duration of each patch, see Equation (4.1)-(4.8), are unchanged from the original model but with an added atrial septal wall patch. As the model still implement one patch for each myocardial wall, the contraction is uniform throughout the atrial septal wall. The atrial septal wall activation time, t_{SAW} is set equal to the left atrial activation time and the duration is set equal to both atrial free walls t_a,

$$t_{SAW} = t_{LAW} \tag{5.1}$$

$$t_a = 0.1765 t_{CC}. \tag{5.2}$$

The inclusion of the atrial three-wall segment in the model result in a smaller change in the course of event of solving the differential equation of each heart beat, see Figure 4.3. The atrial chamber model is removed from the simulation and replaced by an additional execution of the ventricular three-wall segment model for the atria. The theory of this execution has already been presented in Section 4.4.3. The only changes applied are changes in the calculations of cross-section area A and wave impedance Z, which is adapted for both atria and ventricle. The new calculations, which replace Equation (4.34) and (4.35) of the theory are,

$$\begin{cases} A_{LA} = \dfrac{V_{LA} + 0.1V_{LAW} + 0.1V_{SAW}}{2(V_{LA} + 0.5V_{LAW} + 0.5V_{SAW})^{1/3}} \\ A_{RA} = \dfrac{V_{RA} + 0.1V_{RAW} + 0.1V_{SAW}}{2(V_{RA} + 0.5V_{RAW} + 0.5V_{SAW})^{1/3}} \end{cases} \tag{5.3}$$

and,

$$\begin{cases} Z_{LA} = \dfrac{0.2\sqrt{2\rho(V_{LA} + 0.5V_{LAW} + 0.5V_{SAW})^{1/3}\left|\dfrac{dT}{dA}\right|}}{A_{LA}} \\ Z_{RA} = \dfrac{0.2\sqrt{2\rho(V_{RA} + 0.5V_{RAW} + 0.5V_{SAW})^{1/3}\left|\dfrac{dT}{dA}\right|}}{A_{RA}} \end{cases} \tag{5.4}$$

for the atria and similarly,

$$\begin{cases} A_{LV} &= \dfrac{V_{LV} + 0.1V_{LW} + 0.1V_{SW}}{2(V_{LV} + 0.5V_{LW} + 0.5V_{SW})^{1/3}} \\ A_{RV} &= \dfrac{V_{RV} + 0.1V_{RW} + 0.1V_{SW}}{2(V_{RV} + 0.5V_{RW} + 0.5V_{SW})^{1/3}} \end{cases} \tag{5.5}$$

and,

$$\begin{cases} Z_{LV} &= \dfrac{0.2\sqrt{2\rho(V_{LV} + 0.5V_{LW} + 0.5V_{SW})^{1/3}\left|\dfrac{dT}{dA}\right|}}{A_{LV}} \\ Z_{RV} &= \dfrac{0.2\sqrt{2\rho(V_{RV} + 0.5V_{RW} + 0.5V_{SW})^{1/3}\left|\dfrac{dT}{dA}\right|}}{A_{RV}} \end{cases} \tag{5.6}$$

for the ventricles. This change is executed to have the calculations correspond geometrically to the atrial chamber model calculations that are interpreted to be more accurate.

5.2 Radial cylindrical three-wall segment model

The cylindrical three-wall segment model is a model adaptation executed on the ventricles to enable longitudinal and radial pumping. The ventricular model representation is changed to describe the ventricles as a joint cylindrical segment of two cavities enclosed and separated by three myocardial walls. The geometry is constructed by letting a cross-section of the spherical three-wall segment be the base of the cylinder and applying a fixed height z equal to all three ventricular walls, see Figure 5.2. Since the height is fixed, the model only implement radial pumping by modeling myocardial contraction of the cylinder base.

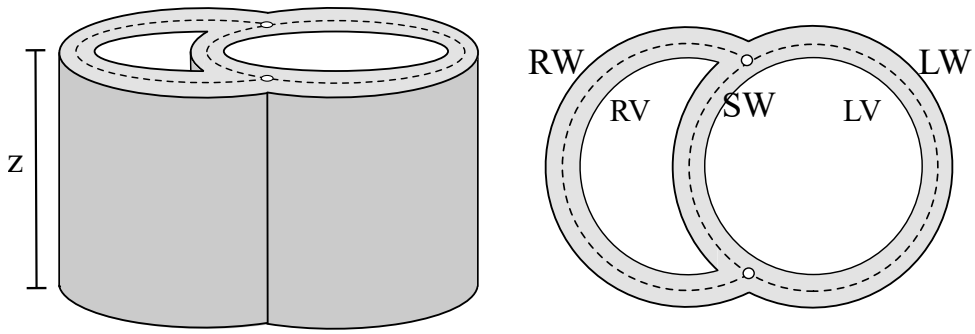

Figure 5.2: A graphical representation of the cylindrical three-wall segment. The base of the cylinder is geometrically equal to a cross-section of the spherical three-wall segment. The height z of the cylinder is a fixed parameter and equal to all three walls. The segment representation is the same as for the original ventricular model with the left (LV) and right (RV) cavity enclosed within a left (LW) and right (RW) ventricular free wall and a septal wall (SW).

5.2.1 Model parameters and state variables

To minimize the changes from the previous model and the spherical representation of the ventricles, the wall volumes and non-contractile areas of all three ventricular walls are unchanged from the original model, see Table A.4 and A.7. Furthermore all myocardial material parameters used to model sarcomere contraction are unchanged for all three walls, see Table A.5. The height parameter z is determined by assuming an unchanged initial state of the left midwall volume. The reference midwall area A_{mRef} is determined by assuming a reference segment base geometry, equal to the original model reference segment cross-section. The adapted parameter values of the cylindrical three-wall segment model are presented in Table 5.3.

DESCRIPTION	LW	SW	RW
Cylinder height	0.0492	0.0492	0.0492
Reference midwall area	$0.64A_{mRef,LW1}$	$0.81A_{mRef,SW1}$	$0.55A_{mref,RW1}$

Table 5.3: Parameters of the cylindrical three-wall segment model for the left ventricular free wall (LW), septal wall (SW) and right ventricular free wall (RW). The new parameter value of A_{mRef} is expressed as a percentage of the original model parameter, presented in Table A.6 of Appendix A.1.

The state variable structure is changed to consider the new geometry of the ventricular segment. The ventricular junction radius y_m is kept as a state variable whereas the previous state variable septal midwall volume $V_{m,SW}$ is replaced by the septal midwall cross-section area of the cylinder base $A_{mC,SW}$. The adapted state variable initial values are presented in Table 5.4.

VARIABLE DESCRIPTION	NOTATION	UNIT	VALUE
Cavity volume	V	LV	$1.0224 \cdot 10^{-4}$
		RV	$5.8127 \cdot 10^{-5}$
Midwall volume	V_m	SW	*removed*
Midwall cross-section area	A_{mC}	SW	0.0011
Junction radius	y_m	Cylinder	0.0347

Table 5.4: Adapted state variable initial values of implementing a cylindrical three-wall segment of the ventricles. The variables are values of the left (LV) and right (RV) ventricles, the septal wall (SW) and the cylindrical segment (Cylinder).

The rest of the state variable initial values are unchanged. The theory of the calculations of the adapted parameter values and state variable initial values are presented in Appendix C.2.

5.2.2 Implementation

The implementation of the cylindrical three-wall segment model change the course of event when solving the differential equation of a heart beat. The ventricular three-wall segment model is replaced by a radial cylindrical three-wall segment model. Similar to the original ventricular model, the cylindrical model determine the cylinder base geometry, the wall tension and transmural pressure of the ventricular walls and cavity cross-section area and wave impedance of the ventricular cavities.

The previously introduced coordinate system, see Figure 5.3, now holds for the cylinder base area. The midwall cross-section area A_{mC} can then be defined as the area of the cylinder base enclosed by the midwall arc length of the corresponding wall and the y-axis.

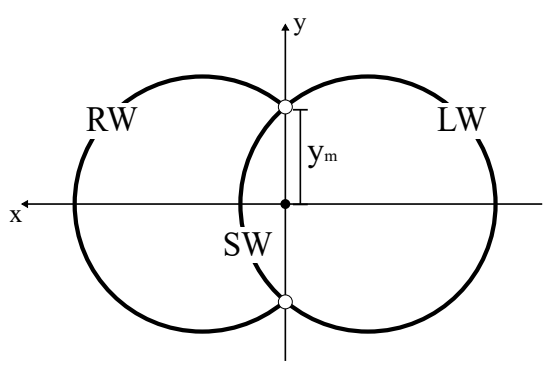

Figure 5.3: A representation of the cylinder base of the cylindrical three-wall segment model. The midwall arc length of each wall are represented as the bold line. The coordinate system is the same as for the spherical three-wall segment model and holds for the cylinder base. y_m is the junction radius. Figure adapted from [21].

Using the septal midwall cross-section area $A_{mC,SW}$ from the preceding time

point, the midwall cross-section area of left $A_{mC,LW}$ and right $A_{mC,RW}$ ventricular free walls can be calculated as,

$$\begin{cases} A_{mC,LW} &= -\dfrac{V_{LV}}{z} - \dfrac{V_{LW}}{2z} - \dfrac{V_{SW}}{2z} + A_{mC,SW} \\ A_{mC,RW} &= \dfrac{V_{RV}}{z} + \dfrac{V_{RW}}{2z} + \dfrac{V_{SW}}{2z} + A_{mC,SW} \end{cases} \tag{5.7}$$

using Equation (4.20) and dividing by the cylinder height z. Note that the definition of a positive and negative midwall cross-section area for the right and left free wall respectively still holds.

Using the midwall cross-section areas and the junction radius y_m from a preceding time point, x_m for each wall can be calculated. From geometry it holds that the midwall cross-section area of the cylinder base can be approximated by,

$$A_{mC} \approx \frac{4}{3} y_m x_m + \frac{x_m^3}{4 y_m} \tag{5.8}$$

which can be written with x_m as the unknown variable as,

$$x_m = \begin{cases} \dfrac{8 \cdot 2^{2/3} y_m^2}{3Q} - \dfrac{2^{1/3} Q}{3} & \text{for RW and SW} \\ \dfrac{2^{1/3} Q}{3} - \dfrac{8 \cdot 2^{2/3} y_m^2}{3Q} & \text{for LW} \end{cases} \tag{5.9}$$

with,

$$Q = \left(\sqrt{729 A_{mC}^2 y_m^2 + 1024 y_m^6} - 27 |A_{mC}| y_m \right)^{1/3}. \tag{5.10}$$

The reason for using an approximation is that the true expression includes an inverse cosine, which affect the speed of the simulation significantly due to the necessity of determining x_m numerically. The approximation used has an accuracy within 0.1% for $0 \leq \alpha \leq 5\pi/12$ and within 0.8% for $5\pi/12 \leq \alpha \leq \pi/2$ [24].

The relations for the midwall surface area A_m and C_m for the new geometry are given by,

$$A_m = \frac{x_m^2 + y_m^2}{x_m} \cos^{-1}\left(\frac{y_m^2 - x_m^2}{x_m^2 + y_m^2} \right) \cdot z \tag{5.11}$$

$$C_m = \frac{2 x_m}{x_m^2 + y_m^2} \tag{5.12}$$

where the midwall surface area is calculated as the midwall arc length times the cylinder height.

The same way as for previous models, the tension T_m of each wall can be calculated as,

$$T_m = \frac{dT}{dA}(A_m - A_{m0}) \tag{5.13}$$

where dT/dA is the time dependent wall area stiffness and A_{m0} is the midwall area at zero tension. From geometry it still holds that the tension x-component T_x and y-component T_y can be expressed as,

$$\begin{cases} T_x &= T_m \cdot \sin(\alpha) \quad \text{with } \sin(\alpha) = \dfrac{2x_m y_m}{x_m^2 + y_m^2} \\ T_y &= T_m \cdot \cos(\alpha) \quad \text{with } \cos(\alpha) = \dfrac{-x_m^2 + y_m^2}{x_m^2 + y_m^2}. \end{cases} \tag{5.14}$$

Note from the coordinate system of the cylinder base that the tension components are located in the cylinder base plane. Using the tension components of each wall, the resultant of the full cylindrical element in the x-direction $T_{x,Cylinder}$ and the y-direction $T_{y,Cylinder}$ can be calculated as,

$$T_{x,Cylinder} = \frac{T_{x,LW} + T_{x,SW} + T_{x,RW}}{\sqrt{T_{m,LW}^2 + T_{m,SW}^2 + T_{m,RW}^2}} \tag{5.15}$$

$$T_{y,Cylinder} = \frac{T_{y,LW} + T_{y,SW} + T_{y,RW}}{\sqrt{T_{m,LW}^2 + T_{m,SW}^2 + T_{m,RW}^2}}. \tag{5.16}$$

Similar to the original CircAdapt model, an estimation of the septal midwall cross-section area $A_{mC,SW}$ and junction radius y_m for each time step can be found using linearization, Newtons method, and the tension derivatives of the full cylinder element. The two variables are estimated as,

$$\begin{cases} y_m^{(k+1)} &= y_m^{(k)} - dY \\ A_{mC,SW}^{(k+1)} &= A_{mC,SW}^{(k)} - dA \end{cases} \tag{5.17}$$

with,

$$\begin{cases} dY &= \dfrac{1}{\det(\mathbf{J}_T)} \Big(\dfrac{dT_{y,Cylinder}}{dA} T_{x,Cylinder}^{(k)} - \dfrac{dT_{x,Cylinder}}{dA} T_{y,Cylinder}^{(k)} \Big) \\ dA &= \dfrac{1}{\det(\mathbf{J}_T)} \Big(- \dfrac{dT_{y,Cylinder}}{dy} T_{x,Cylinder}^{(k)} + \dfrac{dT_{x,Cylinder}}{dy} T_{y,Cylinder}^{(k)} \Big) \end{cases} \tag{5.18}$$

where $\mathbf{J}_T$ is the Jacobian matrix of the tension components. The state variable derivatives are calculated as,

$$\begin{cases} \dot{y}_m &= \dfrac{dY}{\tau} \\ \dot{A}_{mC,SW} &= \dfrac{dA}{\tau} \end{cases} \tag{5.19}$$

for $k = 1$ and τ unchanged from the original model. Setting $k = 1$ from previous time step and repeating the calculations give a converged estimation of the septal

midwall cross-section area and junction radius for the current time step. Executing Equation (5.7)-(5.13) for the updated $A_{mC,SW}$ and y_m give the true A_m, C_m and T_m for each wall for the current time step. Deriving the equation for the transmural pressure p_W from conservation of energy and the new cylindrical geometry give the same equation as for the original model,

$$p_W = 2T_m C_m. \tag{5.20}$$

To consider the flow and hemodynamic properties of the cavities, the cross-section areas and wave impedances of the left and right ventricular cavities are calculated. The cavity cross-section areas A of the cylinder model are given by,

$$\begin{cases} A_{LV} = \dfrac{V_{LV} + 0.1V_{LW} + 0.1V_{SW}}{z} \\ A_{RV} = \dfrac{V_{RV} + 0.1V_{RW} + 0.1V_{SW}}{z} \end{cases} \tag{5.21}$$

and the wave impedances Z are calculated as,

$$\begin{cases} Z_{LV} = \dfrac{0.2\sqrt{\rho z \left|\dfrac{dT}{dA}\right|}}{A_{LV}} \\ Z_{RV} = \dfrac{0.2\sqrt{\rho z \left|\dfrac{dT}{dA}\right|}}{A_{RV}}. \end{cases} \tag{5.22}$$

5.3 Longitudinal cylindrical three-wall segment model

The longitudinal cylindrical three-wall segment model is an extended version of the previous cylindrical model. This model includes longitudinal pumping by introducing the cylinder height z as a state variable. Thus the model simulate radial pumping, due to contraction of the cylinder base, and longitudinal pumping due to contraction of the cylinder height, see Figure 5.4.

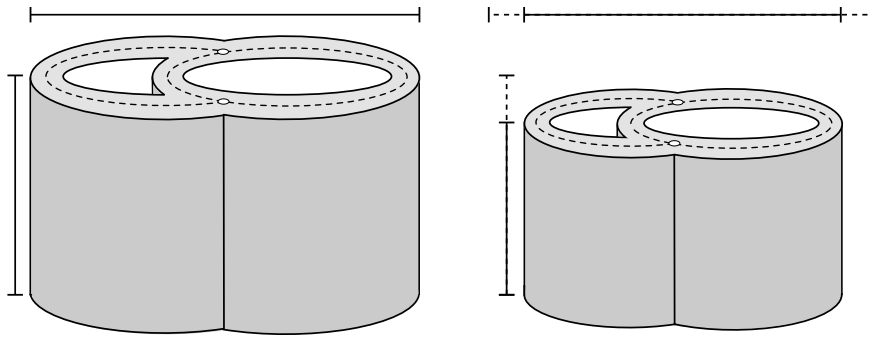

Figure 5.4: A graphical representation of the cylindrical three-wall segment with longitudinal and radial contraction. The figure show cylinder segment dimensions at relaxation (left panel) and at contraction (right panel).

5.3.1 Model parameters and state variables

The wall volumes and non-contractile areas of all three ventricular walls are unchanged from the original model, see Table A.4 and A.7. Furthermore all myocardial material parameters used to model sarcomere contraction are unchanged for all three walls, see Table A.5. The reference midwall area parameter A_{mRef} is calculated identically to the previous radial cylindrical model. The adapted parameter values of the longitudinal cylindrical three-wall segment model are presented in Table 5.5.

DESCRIPTION	LW	SW	RW
Reference midwall area	$0.64A_{mRef,LW1}$	$0.81A_{mRef,SW1}$	$0.55A_{mref,RW1}$

Table 5.5: Parameters of the longitudinal cylindrical three-wall segment model for the left ventricular free wall (LW), septal wall (SW) and right ventricular free wall (RW). The new parameter value of A_{mRef} is expressed as a percentage of the original model parameter, presented in Table A.6 of Appendix A.1.

The longitudinal cylindrical model induce some changes of the state variables, presented for the original model in Table 4.2. As the model include longitudinal contraction, the cylinder height z is considered a state variable, whose initial value is equal to the parameter value of the previous cylindrical model, see Table 5.3. The junction radius variable y_m is still a state variable with unchanged initial value, whereas the septal midwall volume $V_{m,SW}$ of the original three-wall segment model is replaced by the septal midwall cross-section area $A_{mC,SW}$. This model construction increase the number of state variables from 30 to 31. The adapted state variable initial values are presented in Table 5.6.

VARIABLE DESCRIPTION	NOTATION	UNIT	VALUE
Cavity volume	V	LV	$1.0224 \cdot 10^{-4}$
		RV	$5.8127 \cdot 10^{-5}$
Midwall volume	V_m	SW	*removed*
Midwall cross-section area	A_{mC}	SW	0.0011
Junction radius	y_m	Cylinder	0.0347
Cylinder height	z	Cylinder	0.0492

Table 5.6: Adapted state variable initial values of implementing a longitudinal cylindrical three-wall segment of the ventricles. The variables are values of the left (LV) and right (RV) ventricles, the septal wall (SW) and the cylindrical segment (Cylinder).

The rest of the state variable initial values are unchanged. Calculation of the adapted initial values are identical to the calculations executed for the previous cylindrical model presented in Appendix C.2.

5.3.2 Implementation

The implementation of a cylindrical ventricular segment with both radial and longitudinal contraction is executed by replacing the ventricular three-wall segment model by a longitudinal cylindrical three-wall segment model. Similar to the original model, the longitudinal cylindrical model determine cylinder segment geometry, tension and transmural pressure of the three ventricular walls and cross-section area and wave impedance of the two cavities.

Given the septal midwall cross-section area $A_{mC,SW}$ and cylinder height z estimated from the previous time step, the midwall cross-section area of the cylinder base of the left $A_{mC,LW}$ and right $A_{mC,RW}$ ventricular walls can be calculated as,

$$\begin{cases} A_{mC,LW} &= -\dfrac{V_{LV}}{z} - \dfrac{V_{LW}}{2z} - \dfrac{V_{SW}}{2z} + A_{mC,SW} \\ A_{mC,RW} &= \dfrac{V_{RV}}{z} + \dfrac{V_{RW}}{2z} + \dfrac{V_{SW}}{2z} + A_{mC,SW}. \end{cases} \tag{5.23}$$

Notice that a positive midwall cross-section area is defined as the midwall boundary being convex to the positive x-axis. Using the midwall cross-section areas and the joint junction radius y_m, the midwall x-coordinate x_m can be calculated. The cylinder base area approximation,

$$A_{mC} \approx \frac{4}{3} y_m x_m + \frac{x_m^3}{4y_m} \tag{5.24}$$

is used and has the solution,

$$x_m = \begin{cases} \dfrac{8 \cdot 2^{2/3} y_m^2}{3Q} - \dfrac{2^{1/3} Q}{3} & \text{for RW and SW} \\ \dfrac{2^{1/3} Q}{3} - \dfrac{8 \cdot 2^{2/3} y_m^2}{3Q} & \text{for LW} \end{cases} \tag{5.25}$$

with,

$$Q = \left(\sqrt{729A_{mC}^2 y_m^2 + 1024 y_m^6} - 27|A_{mC}|y_m\right)^{1/3}. \quad (5.26)$$

After determining x_m, the midwall surface area A_m and the cylindrical wall curvature C_m can be calculated as,

$$A_m = \frac{x_m^2 + y_m^2}{x_m} \cos^{-1}\left(\frac{y_m^2 - x_m^2}{x_m^2 + y_m^2}\right) \cdot z \quad (5.27)$$

$$C_m = \frac{2x_m}{x_m^2 + y_m^2}. \quad (5.28)$$

The same way as for previous models, the wall tension T_m of each wall is given by,

$$T_m = \frac{dT}{dA}(A_m - A_{m0}) \quad (5.29)$$

where dT/dA is the wall area stiffness and A_{m0} is the midwall surface area at zero tension.

Given the tension T_m of each wall, a three dimensional coordinate system is introduced so that the tension can be divided into three components, see Figure 5.5. The tension x-component T_x and y-component T_y are set, equal to the radial cylindrical model, along the x-axis and y-axis placed on the base of the cylinder segment. The tension z-component T_z is set along the z-axis placed parallel to the height of the cylinder.

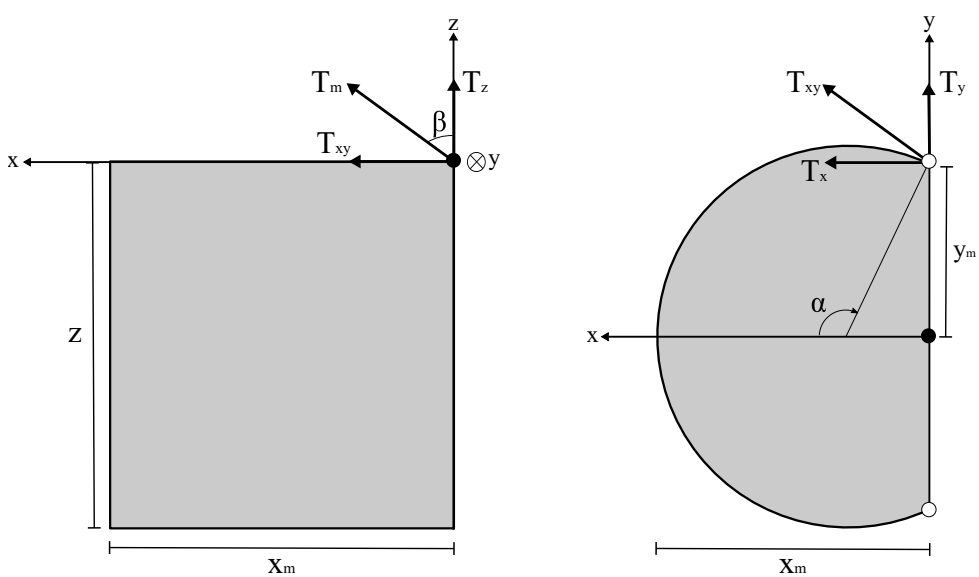

Figure 5.5: A graphical representation of the coordinate system introduced for the longitudinal cylindrical model. Origo of the coordinate system is depicted as the black dot in both figures. The coordinate system is rotated so that the z-axis coincide with the height of the cylinder. The x-axis and y-axis are placed, similar to the original model, to coincide with the cylinder base.

Given the introduced coordinate system, the tension components T_z and T_{xy} are calculated as,

$$\begin{cases} T_{xy} & = T_m \cdot \sin(\beta) \\ T_z & = T_m \cdot \cos(\beta) \end{cases} \tag{5.30}$$

where,

$$\beta = \begin{cases} 2\tan^{-1}\left(\dfrac{x_m^2 + y_m^2}{z}\right) & \text{for SW} \\ -2\tan^{-1}\left(\dfrac{y_m^2(x_m^2 + y_m^2)}{x_m^2 z}\right) & \text{for LW and RW.} \end{cases} \tag{5.31}$$

Further, the tension components T_x and T_y are calculated as components of T_{xy} as,

$$\begin{cases} T_x & = T_{xy} \cdot \sin(\alpha) \quad \text{with } \sin(\alpha) = \dfrac{2x_m y_m}{x_m^2 + y_m^2} \\ T_y & = T_{xy} \cdot \cos(\alpha) \quad \text{with } \cos(\alpha) = \dfrac{-x_m^2 + y_m^2}{x_m^2 + y_m^2}. \end{cases} \tag{5.32}$$

Using the tension components of each wall, the resultant x-component $T_{x,Cylinder}$, y-component $T_{y,Cylinder}$ and z-component $T_{z,Cylinder}$ of the full cylindrical segment are calculated as,

$$T_{x,Cylinder} = \frac{T_{x,LW} + T_{x,SW} + T_{x,RW}}{\sqrt{T_{m,LW}^2 + T_{m,SW}^2 + T_{m,RW}^2}} \tag{5.33}$$

$$T_{y,Cylinder} = \frac{T_{y,LW} + T_{y,SW} + T_{y,RW}}{\sqrt{T_{m,LW}^2 + T_{m,SW}^2 + T_{m,RW}^2}} \tag{5.34}$$

$$T_{z,Cylinder} = \frac{T_{z,LW} + T_{z,SW} + T_{z,RW}}{\sqrt{T_{m,LW}^2 + T_{m,SW}^2 + T_{m,RW}^2}}. \tag{5.35}$$

Recalling that the tension components are functions of the junction radius, septal midwall cross-section area and cylinder height, new estimations for the three state variables are calculated using Newtons method for three dimensions. The new estimates $k+1$ are given by,

$$\begin{cases} y_m^{(k+1)} & = y_m^{(k)} - dY \\ A_{mC,SW}^{(k+1)} & = A_{mC,SW}^{(k)} - dA \\ z^{(k+1)} & = z^{(k)} - dZ \end{cases} \tag{5.36}$$

where,

$$\begin{cases} dY &= \frac{1}{\det(\mathbf{J}_T)}\left(a_{11}T^{(k)}_{x,Cylinder} + a_{12}T^{(k)}_{y,Cylinder} + a_{13}T^{(k)}_{z,Cylinder}\right) \\ dA &= \frac{1}{\det(\mathbf{J}_T)}\left(a_{21}T^{(k)}_{x,Cylinder} + a_{22}T^{(k)}_{y,Cylinder} + a_{23}T^{(k)}_{z,Cylinder}\right) \\ dZ &= \frac{1}{\det(\mathbf{J}_T)}\left(a_{31}T^{(k)}_{x,Cylinder} + a_{32}T^{(k)}_{y,Cylinder} + a_{33}T^{(k)}_{z,Cylinder}\right) \end{cases} \tag{5.37}$$

and

$$a_{11} = \frac{dT_{y,Cylinder}}{da}\cdot\frac{dT_{z,Cylinder}}{dz} - \frac{dT_{y,Cylinder}}{dz}\cdot\frac{dT_{z,Cylinder}}{da} \tag{5.38}$$

$$a_{12} = \frac{dT_{z,Cylinder}}{da}\cdot\frac{dT_{x,Cylinder}}{dz} - \frac{dT_{x,Cylinder}}{da}\cdot\frac{dT_{z,Cylinder}}{dz} \tag{5.39}$$

$$a_{13} = \frac{dT_{x,Cylinder}}{da}\cdot\frac{dT_{y,Cylinder}}{dz} - \frac{dT_{y,Cylinder}}{da}\cdot\frac{dT_{x,Cylinder}}{dz} \tag{5.40}$$

$$a_{21} = \frac{dT_{z,Cylinder}}{dy}\cdot\frac{dT_{y,Cylinder}}{dz} - \frac{dT_{y,Cylinder}}{dy}\cdot\frac{dT_{z,Cylinder}}{dz} \tag{5.41}$$

$$a_{22} = \frac{dT_{x,Cylinder}}{dy}\cdot\frac{dT_{z,Cylinder}}{dz} - \frac{dT_{z,Cylinder}}{dy}\cdot\frac{dT_{x,Cylinder}}{dz} \tag{5.42}$$

$$a_{23} = \frac{dT_{y,Cylinder}}{dy}\cdot\frac{dT_{x,Cylinder}}{dz} - \frac{dT_{x,Cylinder}}{dy}\cdot\frac{dT_{y,Cylinder}}{dz} \tag{5.43}$$

$$a_{31} = \frac{dT_{y,Cylinder}}{dy}\cdot\frac{dT_{z,Cylinder}}{da} - \frac{dT_{y,Cylinder}}{da}\cdot\frac{dT_{z,Cylinder}}{dy} \tag{5.44}$$

$$a_{32} = \frac{dT_{x,Cylinder}}{da}\cdot\frac{dT_{z,Cylinder}}{dy} - \frac{dT_{x,Cylinder}}{dy}\cdot\frac{dT_{z,Cylinder}}{da} \tag{5.45}$$

$$a_{33} = \frac{dT_{x,Cylinder}}{dy}\cdot\frac{dT_{y,Cylinder}}{da} - \frac{dT_{x,Cylinder}}{da}\cdot\frac{dT_{y,Cylinder}}{dy} \tag{5.46}$$

are the elements of the adjugate matrix of the Jacobian $\mathbf{J}_T$. The state variable derivatives are calculated as,

$$\begin{cases} \dot{y}_m &= \frac{dY}{\tau} \\ \dot{A}_{mC,SW} &= \frac{dA}{\tau} \\ \dot{z} &= \frac{dZ}{\tau} \end{cases} \tag{5.47}$$

using Equation (5.37) for $k = 1$ and the parameter τ given in Table A.4. Executing the Newton iterations for $k = 1$ from the previous time step until variable convergence give the new estimated state variables. Using the converged estimations of y_m, $A_{mC,SW}$ and z, Equation (5.23)-(5.29) are executed again. The final tension

T_m and midwall curvature C_m of each wall are used to calculate the transmural pressure p_W,

$$p_W = 2T_m C_m. \tag{5.48}$$

Finally the cross-section areas A of the two cavities are given by,

$$\begin{cases} A_{LV} = \dfrac{V_{LV} + 0.1V_{LW} + 0.1V_{SW}}{z} \\ A_{RV} = \dfrac{V_{RV} + 0.1V_{RW} + 0.1V_{SW}}{z} \end{cases} \tag{5.49}$$

and the wave impedance Z is calculated as,

$$\begin{cases} Z_{LV} = \dfrac{0.2\sqrt{\rho z \left|\dfrac{dT}{dA}\right|}}{A_{LV}} \\ Z_{RV} = \dfrac{0.2\sqrt{\rho z \left|\dfrac{dT}{dA}\right|}}{A_{RV}}. \end{cases} \tag{5.50}$$

Chapter 6

Results

The results presented are simulations and calculations executed on the original CircAdapt model or adapted models of one or several adaptations, presented in Section 5. All results presented have been executed by model simulation with mean arterial pressure p_0 and cardiac output q_0 set to default values, see Table A.1. The cardiac cycle time t_{CC} is set within a range resulting in simulation stability and physiological relevance for a healthy subject at rest.

6.1 Original CircAdapt model

The execution time for the original CircAdapt model with default input parameters is,

$$14.322 \text{ s.} \tag{6.1}$$

The original CircAdapt model is stable for cardiac cycle times,

$$0.6 \leq t_{CC} \leq 1.5 \text{ s.} \tag{6.2}$$

Due to physiology, a wider range of cardiac cycle time has not been analyzed for any of the implemented models.

The total heart volume for default cardiac cycle time is presented in Figure 6.1. The total heart volume variation, collected from the first of the two cycles, is 20.4%.

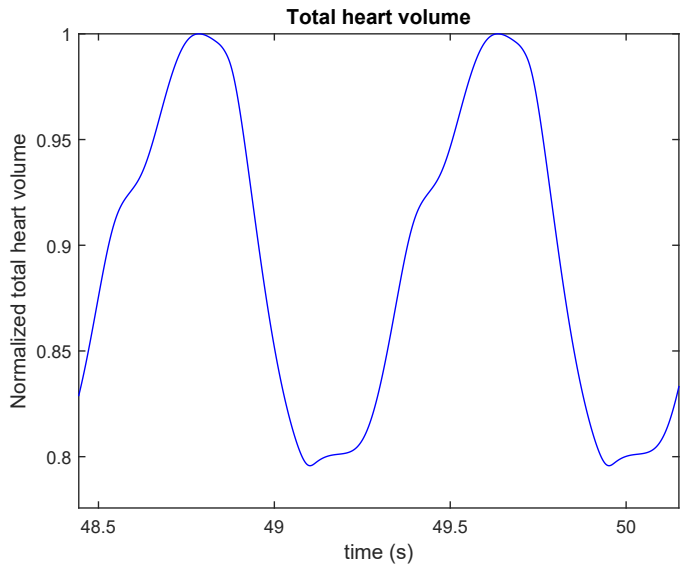

Figure 6.1: Total heart volume of the original CircAdapt model. The figure depict the last two heart beats of a simulation of 50 seconds for default cardiac cycle time, $t_{CC} = 0.85$ s. The plot is normalized to the end diastolic volume.

6.2 Atrial three-wall segment model

This section present results of execution of the original CircAdapt model adapted using the atrial three-wall segment model. The execution time of the adapted model with default input parameters is,

$$19.302 \text{ s}. \tag{6.3}$$

Executions result in stability for cardiac cycle times,

$$0.78 \leq t_{CC} \leq 1.5 \text{ s}. \tag{6.4}$$

The total heart volume for default cardiac cycle time is presented in Figure 6.2. The total heart volume variation, collected from the first of the two cycles, is 19.7%. Wigger diagrams of the left and right side of the heart are presented for the lower stability limit, the default value and the upper stability limit of the cardiac cycle time in Figure 6.3.

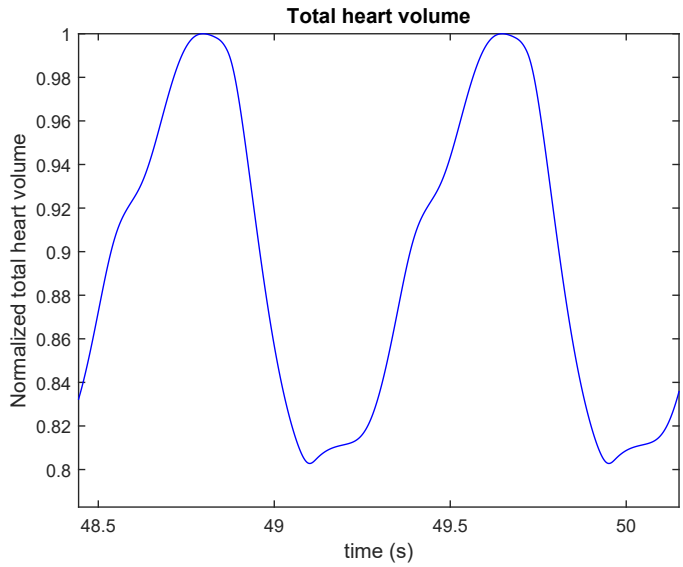

Figure 6.2: Total heart volume of the atrial adapted model. The figure depict the last two heart beats of a simulation of 50 seconds for default cardiac cycle time, $t_{CC} = 0.85$s. The plot is normalized to the end diastolic volume.

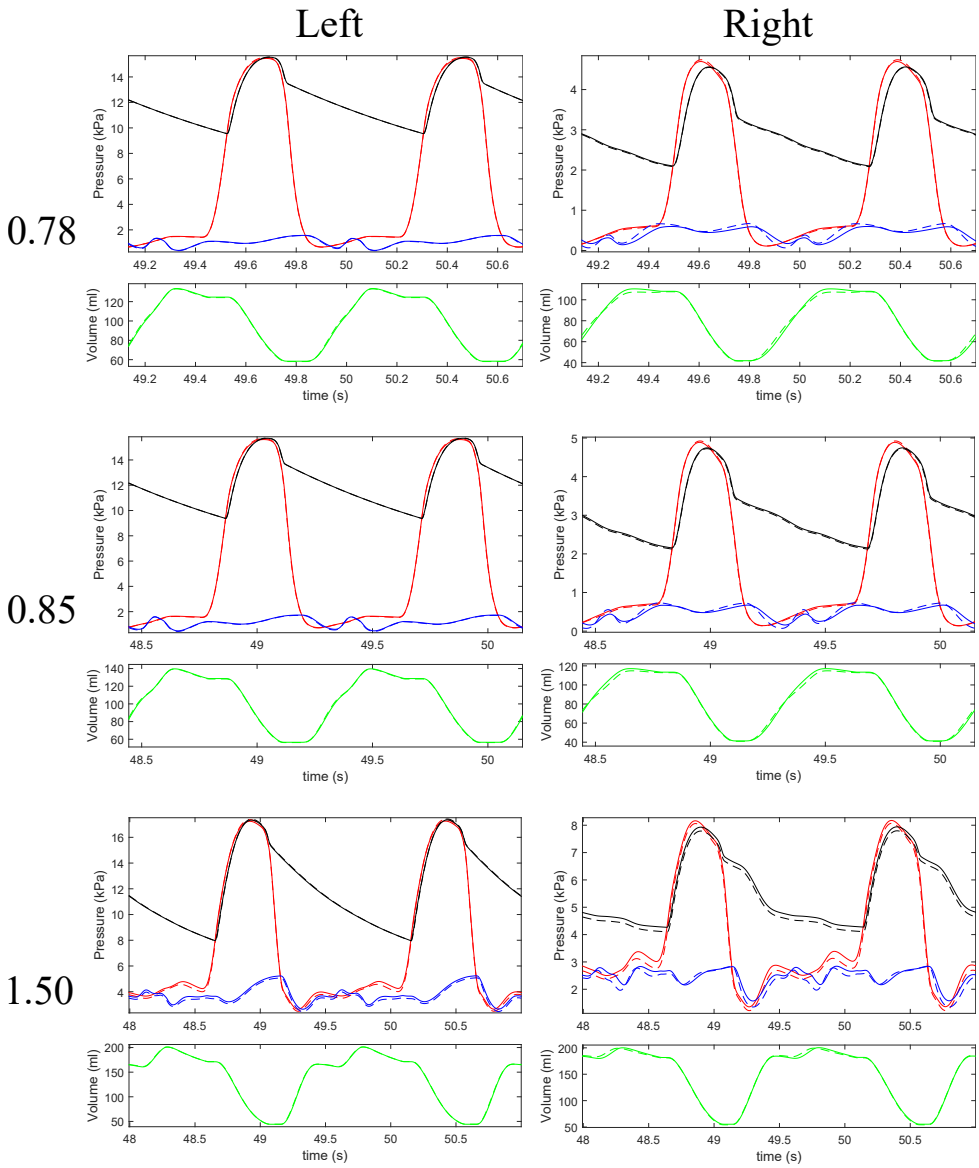

Figure 6.3: Wigger diagram of the model including atrial segment adaptation. The left (left panel) and right (right panel) side of the heart is depicted for cardiac cycle time $t_{CC} = 0.78$s (first row), $t_{CC} = 0.85$s (second row) and $t_{CC} = 1.5$s (third row). The original model is depicted as dashed lines and the adapted model as solid lines. The upper plot of each figure show aortic or pulmonary arterial pressure (black), left or right ventricular pressure (red) and left or right atrial pressure (blue). The lower plot of each figure show the left or right ventricular blood volume (green). The figures show the last two heartbeats of a simulation of 50 seconds. The axes are not scaled to mean aortic pressure or cardiac output.

6.3 Atrial three-wall segment model & Radial cylindrical three-wall segment model

This section present results of execution of the original CircAdapt model adapted using both the atrial three-wall segment model and the radial cylindrical ventricular model. The execution time of the adapted model, with default input parameters is,

$$19.465 \text{ s}. \tag{6.5}$$

The execution is stable for cardiac cycle times,

$$0.73 \leq t_{CC} \leq 1.5 \text{ s}. \tag{6.6}$$

The total heart volume for default cardiac cycle time is presented in Figure 6.4. The total heart volume variation, collected from the first of the two heart beats, is 22.6%. Wigger diagrams of the left and right side of the heart are presented for the lower stability limit, the default value and the upper stability limit of the cardiac cycle time in Figure 6.5.

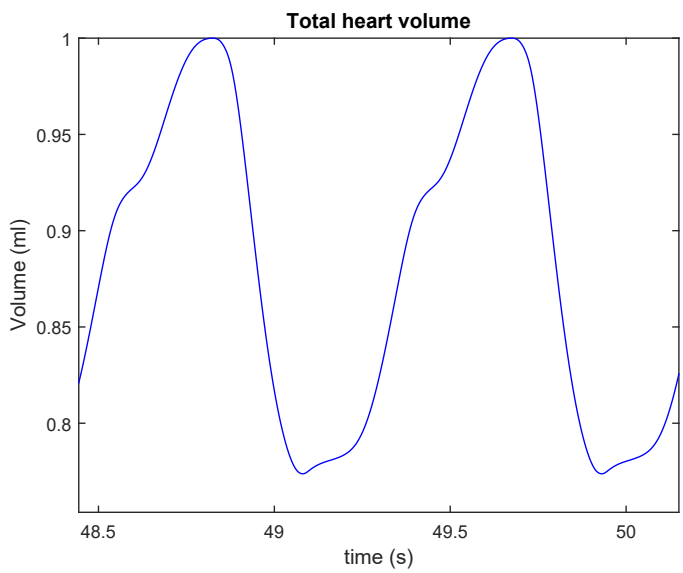

Figure 6.4: Total heart volume of the model adapted to the atrial segment and the radial cylindrical ventricular model. The figure depict the last two heart beats of a simulation of 50 seconds for default cardiac cycle time, $t_{CC} = 0.85$s. The plot is normalized to the end diastolic volume.

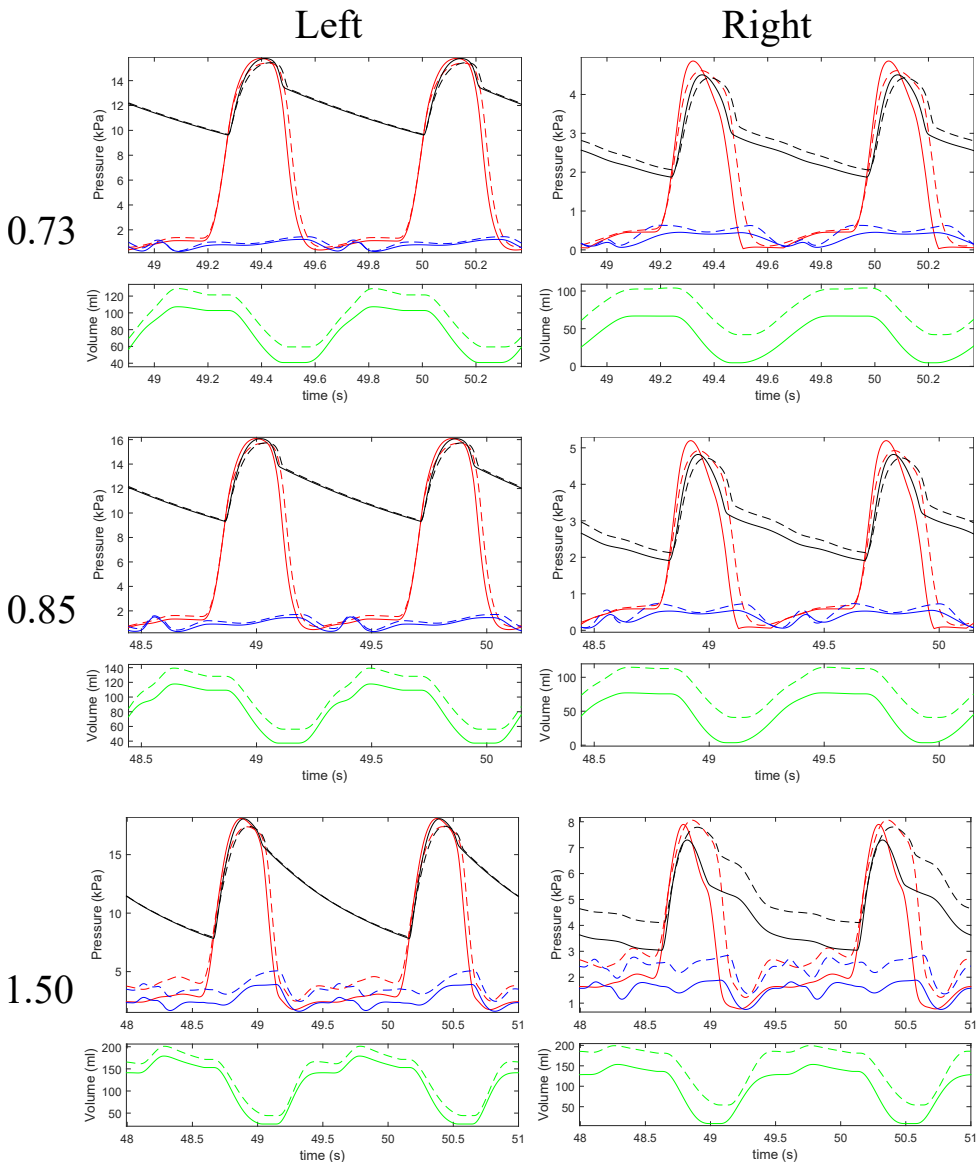

Figure 6.5: Wigger diagram of the model including atrial segment adaptation and radial cylindrical ventricular adaptation. The left (left panel) and right (right panel) side of the heart is depicted for cardiac cycle time $t_{CC} = 0.73$s (first row), $t_{CC} = 0.85$s (second row) and $t_{CC} = 1.5$s (third row). The original model is depicted as dashed lines and the adapted model as solid lines. The upper plot of each figure show aortic or pulmonary arterial pressure (black), left or right ventricular pressure (red) and left or right atrial pressure (blue). The lower plot of each figure show the left or right ventricular blood volume (green). The figures show the last two heartbeats of a simulation of 50 seconds. The axes are not scaled to mean aortic pressure or cardiac output.

6.4 Atrial three-wall segment model & Longitudinal cylindrical three-wall segment model

Execution of the original model with adaptations of both the atrial three-wall segment model and the longitudinal cylindrical ventricular model have been attempted. This model adaptation is unstable for cardiac cycle times within the range of physiological relevance. Potential causes of this is described in the discussion section.

Chapter 7

Discussion

The original CircAdapt model could profit from adaptations that, when implemented, improve the model in general, improve already existing modules or include more components. As discussed shortly in Section 4.6, the adaptations implemented within this thesis only attend a subset of identified limitations and difficulties of the original model. The model in general is well constructed and cover the most significant parts of the cardiovascular system. It also includes and regard known physiological aspects that are important to derive physical properties over the cardiac cycle. Thus the model is relevant and sufficient for the CircAdapt model to be used for educational purposes.

Before considering changes purely for the purpose of physiological accuracy, it is important to consider the limitations rising simply by describing the cardiovascular system as a mathematical system of differential equations. A general challenge in biomedical modeling is the aim for numerical stability, and the CircAdapt model is no exception. This has to do with both model equations and model parameters. Implemented equations are often a trade off between accuracy and model complexity. As declared by Theo Arts and Joost Lumens of the CircAdapt Research Team, certain approximations are introduced as one prefers numerical stability over the highest accuracy [25]. Simple equations are often in need of few parameters with a higher risk of instability, whereas complex models attend stability better but could be unmanageable as the calculations become difficult to handle due to too many unknowns. Another effect that have occurred during this thesis is that even when choosing well motivated and derived parameters that are theoretically relevant, the simulation might be unstable. The drive towards stability is also more complex than finding a model setup that is stable for the differential equations modeling a heart beat. The model simulate a dynamical system which is why it is of great significance to also reach stability over a longer sequence of heart beats.

As Section 4.6 present there are physiological model limitations in the structure and modeling of blood vessels, myocardial walls and valves. Larger vessels include more layers of connective tissue and smooth muscle cells than smaller ves-

sels [1]. Therefore future work should consider more blood vessel components as the material properties included in the model, such as wall stiffness, may vary with vessel size. The simplifications of the blood vessels are however reasonable, as the present focus of the CircAdapt model is simulation of the heart. An adaptation to the myocardial model, already suggested and implemented in theory by the CircAdapt Research Team, is to include several patches within a myocardial wall. The source code is currently implementing several patches, but as the number of patches is set to one it does not affect the final result. As suggested by the CircAdapt Research Team, several patches would provide the ability to model activation time and tissue properties differently between patches within the same myocardial wall [22]. This would be an important property of cardiovascular modeling when modeling the diseased heart, for example for patients with abnormalities in myocardial action potential activation or patients suffering from a heart attack. The current version of CircAdapt implement one set of sarcomeres, an approximation that is sufficient when modeling spherical segments as they contract radially. When introducing the adaptation of a radially and longitudinally contracting cylindrical ventricle however, improving the sarcomere mechanics model becomes more important. As have been shown by dissection, sarcomeres within the ventricular myocardium show gradual rotation both from the outer to the inner boundary of the myocardium and from the apex to the AV-plane [10, 14]. When introducing longitudinal pumping, differently rotated sarcomeres should be exposed to different amplitudes of radial and longitudinal tension. Thus, adapting the modeling of the sarcomeres is a natural continuation of CircAdapt adaptation as a result of the adaptations executed in this thesis. The modeling of the valves is quite accurate as it includes several states determined by a pressure-flow relation, that coincide well with what have been shown by Noble [9]. To model atrial inflows, septal defects and PDA as valves is however a substantial simplification that could be improved in future adaptations. An adaptation to the model that would improve its performance in general is to adapt its calculations of myocardial activation over the cardiac cycle, see Equation (4.7)-(4.8). The relation is now modeled as a linear function between diastolic duration and the cardiac cycle time, but has been shown by Chung et al. to correlate very well with a non-linear relationship [23].

Other than the already existing modules of the CircAdapt simulation it would be of interest to expand the model, as it is known from more general physiology that other parts of the body, than the cardiovascular system itself, contribute to its dynamics. Other organ systems, such as the nervous system and the endocrine system, have an ability to affect heart rate, as both sympathetic and parasympathetic nerves and the hormone epinephrine are in connection with the electrical pathway controlling myocardial activation of the right atrium [1]. The closest excluded component however is the thorax, i.e. chest cavity, that have a close correlation to pressure-volume relations of the heart. Including the chest cavity in the CircAdapt model would improve the pericardium model from a physiological perspective, as well as

enabling modeling cardiovascular effects due to respiration. As the respiration cycle affects the pressure within the thorax, the venous flow from the vena cava to the right atrium will adapt due to a change in the pressure gradient. As the pericardium is currently modeled without any outer wall boundary, this would also be modeled more closely to physiology by including a thorax in the model.

7.1 Model adaptations

7.1.1 Atrial three-wall segment model

By analyzing the results of the model implementation of the atrial three-wall segment model it can be seen, from Figure 4.15 and 6.2, that the total heart volume variation decreases a small amount. A small decrease is logical but since no additional outer boundary is applied, a significant decrease is not expected. The ventricles correspond to a larger portion of the total heart volume, and are unchanged for this adaptation. Furthermore, it can be concluded from the adaptation implementation that the sphere-sphere intersection, resulting in the y-axis, made from the is set at a very small portion of each sphere. This is done on purpose after studing atrial geometry on MR-images, however it results in a very small portion of the pump function of the atrium occurring due to the atrial septum. Studing the Wigger diagrams of Figure 6.3 it can be seen that the adaptation induce very little difference to the result. This is positive for the properties of the components regarding the ventricles, but even the atrial pressure is not significantly influenced. The most significant difference occurring with this model adaptation is for the right side of the heart for long cardiac cycle times, $t_{CC} = 1.5$. It can be seen from the full result of this execution however, that the dynamics is not properly stabilized and a longer simulation would be desirable to draw any definite conclusions.

This adaptation of an atrial three-wall segment, compared to the original CircAdapt model can also be seen to have both a longer execution time and a more narrow range of stability. This is important when analyzing the necessity of this adaptation, as biomedical modeling is often a trade off between accuracy and computational demand. The atrial three-wall segment model is more accurate from a physiological perspective, but based on the result presented it does not seem to have an influence on the outcome that compensate for its longer execution time and decreased stability. To draw any conclusions on whether or not this model adaptation is worth executing, compared to the original model, more analysis of the result must be performed. Another important note is that this model took a long time to implement, as the CircAdapt model is sensitive to parameter changes and it took a lot of time to implement a set of parameters and initial values that gave a stable solution to the differential equations. With that said, it has not been concluded that the parameters used are the parameters that provide the best possible solution.

7.1.2 Atrial three-wall segment model & Radial cylindrical three-wall segment model

Analyzing the results of implementing both the atrial three-wall segment model and the radial cylindrical model show an increase in total heart volume variation by 2%. A difference in total heart volume after the adaptation was expected as the geometry of the ventricle has changed. The cylindrical model calculate wall tension by considering a constant cylinder height, whereas the original ventricular model calculate the same tension by considering rotational symmetry. As the tension is used to estimate true segment geometry, a change in total heart volume variation is expected. As no boundary conditions have been applied to the segment contraction, the adaptation is not expected to improve the total heart volume variation.

Studying the Wigger diagrams of Figure 6.5 it can be seen that the model adaptation result in a significant offset in pressure and volume from the original model. The decreased atrial pressure is more significant than for only atrial adaptation, as in Figure 6.3, suggesting that implementing a cylindrical ventricle also affect atrial simulation. From the left column of Figure 6.5 it can be seen that the atrial and ventricular adaptation is quite accurate for the left side of the heart, as both pressure and volume curves follow the dynamical pattern of the original model. Studying the right column, it can be said that there are severe errors in dynamical calculations of the right heart properties. Especially for long cardiac cycle times. As the cylinder height parameter is estimated to match the initial state of the left ventricular wall, it is logical that the largest errors would be in simulating the right ventricle. Further analysis and other sets of right ventricular parameters should be implemented to conclude if the model has potential to perform better for more suitable parameter choices.

The execution time of executing only atrial adaptation, Equation (6.3), do not increase significantly when also implementing the radial cylindrical model, Equation (6.5). This indicate that the radial cylindrical model is not computationally more challenging that the original ventricular three-wall segment model, which is a result supporting further work with this model from a computational work and model complexity point of view. It is also a result supporting future work with the currently unstable longitudinal model, as the radial cylindrical model is not an interesting model in itself but can be expanded to include longitudinal pumping.

7.1.3 Atrial three-wall segment model & Longitudinal cylindrical three-wall segment model

The longitudinal cylindrical segment model is currently unstable. Future work therefore include finding parameters and changing the model implementation to achieve computational stability of the model. Further analysis and debugging of the model implies that the error lies within the initial state of the model and the implemented Newtons method. The Newton method of iterations, currently used to

update the cylindrical segment geometry, is dependent on a three-wall segment that is always under the influence of tension. This is a reasonable assumption physiologically, but it could occur in the current model. As the tension becomes zero in all three walls at the same time step, The Jacobian matrix no longer has an inverse. This inverse is essential for the implemented method and thus the model becomes unstable. This theory also hold for the original spherical three-wall segment model and radial cylindrical segment model, that implement the same iterations. Debugging the MATLAB-code of the atrial three-wall segment model for $t_{CC} = 0.77$ suggest that this theory is in fact what causes instability for cardiac cycle times outside of the stability range, both for the atrial segment model and the radial cylindrical model. Taking this into consideration, finding parameter values that assure tension in at least one wall could cause stability, or a broader stability range, of the models implementing Newtons method.

Chapter 8

Conclusions

The CircAdapt model is a well constructed model that can be used for educational purposes to simulate the cardiovascular system. The model considers many of the anatomical and physiological properties that exist for the system. It uses physical relations and hemodynamics that are pure mathematical equations, that have been shown to realistically approximate the true course of event in heart and blood vessels. The model have limitations in the aspect of anatomy and physiology, most of which are reasonable when considering the trade of between stability, accuracy and model complexity.

Adapting an already existing model is quite difficult. One must consider and understand the full model implementation and construct a model adaptation that function with the rest of the model. Writing the programming code that enable a simulation was, in this thesis project, quite easy, compared to finding suitable parameters. The parameters used in the adaptations were determined partially by geometrical calculations and partially by trial and error. These methods are a combination of what is concluded the most difficult part of cardiovascular modeling, to construct a model of both physiological relevance and numerical stability.

Depending on the focus, the severity of each model limitation may vary. In this thesis, the atrial and ventricular anatomical representation, as well as the absence of ventricular longitudinal pumping, were set as the main focus of model adaptation. The three adapted models are all improving anatomy or physiology of the heart, but could benefit from additional work to increase accuracy and stability.

Chapter 9

Future work

Further adaptations of the CircAdapt model should advance the model representation of heart anatomy and cardiac pumping physiology. The main goal of the thesis adaptations are not the adaptations themselves but rather how they can be used in future work to achieve a model with longitudinal pumping and decreased total heart volume variation, that more closely resemble what is known from MR-image analysis. The result of future work should model both atria and ventricles with improved geometry, that allows longitudinal and radial pumping to be modeled separately. An example of this can be seen in Figure 9.1. Furthermore the total heart volume variation could be decreased by connecting the longitudinal pumping of the atrial segment to the longitudinal pumping of the ventricular segment using boundary conditions.

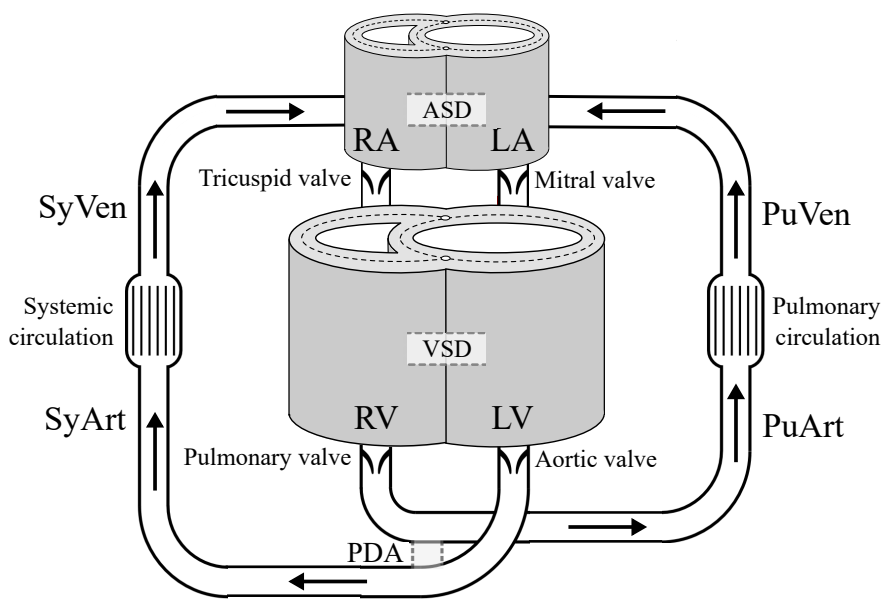

Figure 9.1: A schematic presentation of a future adapted CircAdapt model. Figure adapted from [16].

Before moving forward with additional adaptations, the three adaptations executed should be improved and validated. The Newton iteration method is limited, as wall tension is required. This requirement is reasonable but increase the demand put upon the model parameters. Newtons method also requires the same number of tension components as iteration variables, which might not be desirable for modeling the heart. Therefore, a different method might be preferable.

As stability of both the heart beat dynamics and the heart beat sequence is a significant limitation of the model, future work should aim towards a larger range of stability. An alternate modeling language could be considered to evaluate and improve this. Even though many suggestions of improvement have been made, it is important to remember for any future work, validation or further development, that the model is sensitive to changes. To increase the models field of application it would therefore be crucial to make the model stable and valid for all parameters within the range of physiological relevance. The final long-term goal is a model that can simulate the true cardiac pumping mechanism and where the input parameters are altered to cover subject-specific properties. This way the model could simulate the cardiac cycle dynamics for different patients and not only be used educationally, but also clinically. The model could then hopefully be used as a simulation tool to improve health care and to identify optimal, patient-specific treatment.

Bibliography

[1] Eric P. Widmaier, Hershel Raff, Kevin T. Strang. *Vander's Human Physiology, The Mechanism of Body Function*. McGraw-Hill Education, 2016.

[2] World Health Organization WHO, Cardiovascular Diseases (CVD's), http://www.who.int/mediacentre/factsheets/fs317/en/. Accessed date: 2017-03-27.

[3] Global Health Estimates 2015: Deaths by Cause, Age, Sex, by Country and by Region, 2000-2015. Geneva, World Health Organization; 2016.

[4] Hjärt-lungfonden, Hjärt- och kärlsjukdomar, https://www.hjart-lungfonden.se/Sjukdomar/Hjartsjukdomar/. Accessed date: 2017-03-27.

[5] Hjärt-lungfonden, Hjärtinfarkt, https://www.hjart-lungfonden.se/Sjukdomar/Hjartsjukdomar/Hjartinfarkt/. Accessed date: 2017-03-27.

[6] Aplysia, http://aplysia.se/aplysiacardiovascularlab.htm. Accessed date: 2017-05-17.

[7] CircAdapt, www.circadapt.org. Accessed date: 2017-02-20.

[8] SimVascular, http://simvascular.github.io/. Accessed date: 2017-05-17.

[9] M. I. M. Noble. *The contribution of blood momentum to left ventricular ejection in the dog*. Circulation Research, Journal of the American Heart Association. 1968;23:663-670.

[10] M. Carlsson. *Aspects on Cardiac Pumping*. Department of Clinical Physiology, Lund University, 2007.

[11] M. Carlsson, P. Cain, C. Holmqvist, F. Stahlberg, S. Lundback, H. Arheden. *Total heart volume variation throughout the cardiac cycle in humans*. American Journal of Physiology. Heart and Circulatory Physiology. 2004;287(1):H243-50.

[12] V. Rangarajan, S. J. Chacko, S. Romano, J. Jue, N. Jariwala, J. Chung, A. Farzaneh-Far. *Left ventricular long axis function assessed during cine-cardiovascular magnetic resonance is an independent predictor of adverse cardiac events*. Journal of Cardiovascular Magnetic Resonance. 2016;18:35.

[13] National Heart, Lung and Blood Institute. *What is Patent Ductus Arteriosus?* https://www.nhlbi.nih.gov/health/health-topics/topics/pda. Accessed date: 2017-02-23.

[14] P. Arvidsson. *Physiological aspects on intracardiac blood flow*. Department of Clinical Physiology, Lund University, 2017.

[15] N. Westerhof, n. Stergiopulos, M. I. M. Noble. *Snapshots of hemodynamics - An aid for clinical research and graduate education*. Second edition, Springer Science+Business media, 2010.

[16] *Manual CircAdapt Simulator v1.0.2*, http://www.circadapt.org/documentation. Department of Biomedical Engineering Maastricht University, The Netherlands. Accessed: 2017-01-16.

[17] Arts T, Delhaas T, Bovendeerd P, Verbeek X and Prinzen FW. *Adaptation to mechanical load determines shape and properties of heart and circulation, the CircAdapt model*. American Journal of Physiology. Heart and Circulatory Physiology. 2005;288(4):H1943-54.

[18] MATLAB source code of the CircAdapt Simulator, http://www.circadapt.org/downloads. Accessed: 2017-01-16.

[19] T. Arts, T. Delhaas, F. Prinzen, J. Lumens. *The CircAdapt Model*, http://www.circadapt.org/downloads. Accessed: 2017-01-16.

[20] T. Arts, K. Reesink, W. Kroon, T. Delhaas. *Simulation of adaptation of blood vessel geometry to flow and pressure: Implications for arterio-venous impedance*. Mechanics Research Communications 2012;42:15-21.

[21] J. Lumens, T. Delhaas, B. Kirn, T. Arts. *Three-Wall Segment (TriSeg) Model Describing Mechanics and Hemodynamics of Ventricular Interaction*, Annals of Biomedical Engineering. 2009;37(11):2234-55.

[22] J. Walmsley, T. Arts, N. Derval, P. Bordachar, H. Cochet, S. Ploux, F. W. Prinzen, T. Delhaas, J. Lumens. *Fast simulation of mechanical heterogenety in the electrically asynchronous heart using the MultiPatch module*. PLoS Computational Biology. 2015;11(7):e1004284.

[23] C. S. Chung, M. Karamanoglu, S. J. Kovács. *Duration of diastole and its phases as a function of heart rate during supine bicycle exercise*. American Journal of Physiology. Heart and Circulatory Physiology. 2004;287(5):H2003-8.

[24] E. W. Weisstein. *CRC Concise Encyclopedia of Mathematics*, Second Edition, 2002.

[25] Email correspondence with T. Arts (PhD) and J. Lumens (PhD) of the CircAdapt Research Team.

Appendix A

Tables

A.1 Parameter values of the original CircAdapt model

GENERAL PARAMETERS

PARAMETER DESCRIPTION	NOTATION	VALUE
Blood density [kg/m^3]	ρ	1050
Cardiac cycle time (default value) [s]	t_{CC}	0.85
Cardiac output (default value) [cm^3/s]	q_0	84
Mean aortic pressure (default value) [kPa]	p_0	12.2
Number of heart beats (default value)	N_{HB}	2
Time step length [s]	dt	0.002

Table A.1: General parameters of the original CircAdapt model.

PARAMETERS OF THE BLOOD VESSEL MODEL

PARAMETER DESCRIPTION	NOTATION	UNIT	VALUE
Capillary stiffness	k_{ArtVen}	SyArtVen	1
		PuArtVen	2
Fiber stiffness	k	SyArt	8
		SyVen	10
		PuArt	8
		PuVen	10
Length [m]	l	SyArt	0.4
		SyVen	0.4
		PuArt	0.2
		PuVen	0.2
Reference area [m^2]	A_{Ref}	SyArt	$4.9720 \cdot 10^{-4}$
		SyVen	$4.9830 \cdot 10^{-4}$
		PuArt	$4.6850 \cdot 10^{-4}$

		PuVen	$5.0910 \cdot 10^{-4}$
Reference flow [m^3/s]	$q_{Ref,ArtVen}$	SyArtVen	$4.5 \cdot 10^{-5}$
		PuArtVen	$4.5 \cdot 10^{-5}$
Reference pressure [Pa]	p_{Ref}	SyArt	12164
		SyVen	228
		PuArt	2630
		PuVen	678
Reference pressure drop [Pa]	$p_{Ref,ArtVen}$	SyArtVen	$6.3361 \cdot 10^{3}$
		PuArtVen	1500
Wall cross-section area [m^2]	A_W	SyArt	$1.1370 \cdot 10^{-4}$
		SyVen	$6.4100 \cdot 10^{-5}$
		PuArt	$9.6700 \cdot 10^{-5}$
		PuVen	$5.9500 \cdot 10^{-5}$

Table A.2: Parameter values of the blood vessel model. The parameters show parameters of the systemic (SyArtVen) and pulmonary (PuArtVen) capillary networks. It also show the vessel parameters of the systemic artery (SyArt), systemic vein (SyVen), pulmonary artery (PuArt) and pulmonary vein (PuVen). The parameter $p_{Ref,SyArtVen}$ is presented as its initial value.

PARAMETERS OF THE ATRIAL CHAMBER MODEL

PARAMETER DESCRIPTION	NOTATION	UNIT	VALUE
Wall volume [m^3]	V_W	LAW	$1.3377 \cdot 10^{-5}$
		RAW	$5.4588 \cdot 10^{-6}$

Table A.3: Parameters of the atrial chamber model. The values are given for the left atrial wall (LAW) and the right atrial wall (RAW).

PARAMETERS OF THE VENTRICULAR THREE-WALL SEGMENT MODEL

PARAMETER DESCRIPTION	NOTATION	UNIT	VALUE
Time step scaling parameter [s]	τ	TriSeg	0.001
Wall volume [m^3]	V_W	LW	$1.1382 \cdot 10^{-4}$
		SW	$3.8320 \cdot 10^{-5}$
		RW	$8.0093 \cdot 10^{-5}$

Table A.4: Parameters of the ventricular three-wall segment model. The table present parameters of the left ventricular free wall (LW), septal wall (SW) and right ventricular free wall (RW) as well as parameters of the full three-wall segment (TriSeg).

PARAMETERS OF THE SARCOMERE MECHANICS MODEL

PARAMETER DESCRIPTION	NOTATION	UNIT	VALUE
Activation duration (Default value) [s]	$t_{a/v}$	LAW1	0.15
		RAW1	0.15

		LW1	0.425
		SW1	0.425
		RW1	0.425
Activation time (Default value) [s]	t_W	LAW1	0.0284
		RAW1	0
		LW1	0.3
		SW1	0.3
		RW1	0.3
Active stress parameter [Pa]	$\sigma_{f,act}$	LAW1	60 000
		RAW1	60 000
		LW1	100 000
		SW1	100 000
		RW1	100 000
Decay time parameter [s]	T_D	LAW1	0.4
		RAW1	0.4
		LW1	0.25
		SW1	0.25
		RW1	0.25
Maximum sarcomere shortening velocity [μm/s]	v_{max}	LAW1	14
		RAW1	14
		LW1	7
		SW1	7
		RW1	7
Passive stress parameter [Pa]	$\sigma_{f,pas}$	LAW1	82 928
		RAW1	104 810
		LW1	22 755
		SW1	22 654
		RW1	22 957
Passive stress sarcomere length parameter [μm]	$dL_{s0,pas}$	LAW1	0.6
		RAW1	0.6
		LW1	0.6
		SW1	0.6
		RW1	0.6
Reference sarcomere length [μm]	L_{sRef}	LAW1	2
		RAW1	2
		LW1	2
		SW1	2
		RW1	2
Rise time parameter [s]	T_R	LAW1	0.4
		RAW1	0.4
		LW1	0.25
		SW1	0.25

		RW1	0.25
Sarcomere length at isovolumetric contraction [μm]	$L_{se,iso}$	LAW1	0.04
		RAW1	0.04
		LW1	0.04
		SW1	0.04
		RW1	0.04
Sarcomere length at zero active stress [μm]	L_{si0}	LAW1	1.51
		RAW1	1.51
		LW1	1.51
		SW1	1.51
		RW1	1.51
Sarcomere length at zero passive stress [μm]	$L_{s0,pas}$	LAW1	1.8
		RAW1	1.8
		LW1	1.8
		SW1	1.8
		RW1	1.8

Table A.5: Parameters of the sarcomere mechanics model. The five rows display each parameter for the left atrial wall patch (LAW1), right atrial wall patch (RAW1), left ventricular free wall patch (LW1), septal wall patch (SW1) and right ventricular free wall patch (RW1).

PARAMETERS OF THE MYOCARDIAL PATCH MODEL

PARAMETER DESCRIPTION	NOTATION	UNIT	VALUE
Patch wall volume [m^3]	V_W	LAW1	$1.3377 \cdot 10^{-5}$
		RAW1	$5.4588 \cdot 10^{-6}$
		LW1	$1.1382 \cdot 10^{-4}$
		SW1	$3.8320 \cdot 10^{-5}$
		RW1	$8.0093 \cdot 10^{-5}$
Reference midwall area [m^2]	A_{mRef}	LAW1	0.0071
		RAW1	0.0058
		LW1	0.0099
		SW1	0.0052
		RW1	0.0135

Table A.6: Parameters of the myocardial patch model. The five rows represent the variable value of the left atrial wall patch (LAW1), right atrial wall patch (RAW1), left ventricular free wall patch (LW1), septal wall patch (SW1) and right ventricular free wall patch (RW1).

PARAMETERS OF THE MYOCARDIAL WALLS

PARAMETER DESCRIPTION	NOTATION	UNIT	VALUE
Non-contractile midwall area [m^2]	A_{mDead}	LAW	$6.6176 \cdot 10^{-4}$
		RAW	$6.6176 \cdot 10^{-4}$

LW	0
SW	0
RW	$6.6176 \cdot 10^{-4}$

Table A.7: Additional parameters of the myocardial walls. The five rows present the variable value of the left atrial wall (LAW), right atrial wall (RAW), left ventricular free wall (LW), septal wall (SW) and right ventricular free wall (RW).

PARAMETERS OF THE PERICARDIUM MODEL

PARAMETER DESCRIPTION	NOTATION	VALUE
Reference pressure [Pa]	p_{ref}	1000
Reference volume [m^3]	V_{ref}	$7.2379 \cdot 10^{-4}$
Stiffness exponent	k	10

Table A.8: Parameters of the pericardium model.

PARAMETERS OF THE VALVE FLOW MODEL

PARAMETER DESCRIPTION	NOTATION	UNIT	VALUE
Closed cross-section area [m^2]	A_{leak}	SyVenRa	$2.6471 \cdot 10^{-4}$
		RaRv	$2.6471 \cdot 10^{-10}$
		RvPuArt	$2.6471 \cdot 10^{-10}$
		PuVenLa	$2.6471 \cdot 10^{-4}$
		LaLv	$2.6471 \cdot 10^{-10}$
		LvSyArt	$2.6471 \cdot 10^{-10}$
		LaRa	$2.6471 \cdot 10^{-10}$
		LvRv	$2.6471 \cdot 10^{-10}$
		SyArtPuArt	$2.6471 \cdot 10^{-10}$
Open cross-section area [m^2]	A_{open}	SyVenRa	$4.9811 \cdot 10^{-4}$
		RaRv	$7.0281 \cdot 10^{-4}$
		RvPuArt	$4.6854 \cdot 10^{-4}$
		PuVenLa	$5.0903 \cdot 10^{-4}$
		LaLv	$7.4578 \cdot 10^{-4}$
		LvSyArt	$4.9719 \cdot 10^{-4}$
		LaRa	$2.6471 \cdot 10^{-10}$
		LvRv	$2.6471 \cdot 10^{-10}$
		SyArtPuArt	$2.6471 \cdot 10^{-10}$
Valve length [m]	l	SyVenRa	0.0163
		RaRv	0.0163
		RvPuArt	0.0163
		PuVenLa	0.0163
		LaLv	0.0163
		LvSyArt	0.0163

LaRa	0.0163
LvRv	0.0163
SyArtPuArt	0.0163

Table A.9: Parameters of the valve flow model. The model valves are the right atrium inflow channel (SyVenRa), the tricuspid valve (RaRv), the pulmonary valve (RvPuArt), the left atrium inflow channel (PuVenLa), the mitral valve (LaLv), the aortic valve (LvSyArt), ASD (LaRa), VSD (LvRv) and PDA (SyArtPuArt).

A.2 Initial values of the original CircAdapt model

INITIAL VALUES OF STATE VARIABLES

VARIABLE DESCRIPTION	NOTATION	UNIT	VALUE
Time [s]	t	-	0
Cavity volume [m^3]	V	SyArt	$1.8356 \cdot 10^{-4}$
		SyVen	$2.0111 \cdot 10^{-4}$
		PuArt	$8.5024 \cdot 10^{-5}$
		PuVen	$9.7462 \cdot 10^{-5}$
		LA	$6.3567 \cdot 10^{-5}$
		RA	$4.1467 \cdot 10^{-5}$
		LV	$9.5489 \cdot 10^{-5}$
		RV	$7.9130 \cdot 10^{-5}$
Valve flow [m^3/s]	q	SyVenRa	$1.5898 \cdot 10^{-4}$
		RaRv	$7.8331 \cdot 10^{-5}$
		RvPuArt	$-4.9301 \cdot 10^{-10}$
		PuVenLa	$1.1280 \cdot 10^{-4}$
		LaLv	$4.3784 \cdot 10^{-7}$
		LvSyArt	$-1.1207 \cdot 10^{-9}$
		LaRa	$2.3678 \cdot 10^{-10}$
		LvRv	$2.6180 \cdot 10^{-10}$
		SyArtPuArt	$1.0411 \cdot 10^{-9}$
Contractility	C	LAW1	$9.4085 \cdot 10^{-16}$
		RAW1	$1.5511 \cdot 10^{-16}$
		LW1	$7.1765 \cdot 10^{-5}$
		SW1	$1.0859 \cdot 10^{-4}$
		RW1	$2.6127 \cdot 10^{-5}$
Intrinsic sarcomere length [μm]	L_{si}	LAW1	2.0218
		RAW1	1.8829
		LW1	1.9399
		SW1	1.9738
		RW1	1.8680
Midwall volume [m^3]	V_m	SW	$4.6636 \cdot 10^{-5}$

Junction radius [m]	y_m	TriSeg	0.0347

Table A.10: Initial values of the state variables of the original CircAdapt model.

Appendix B

Derivations

B.1 Blood vessel impedance

The blood vessel model of the CircAdapt model assumes large vessels which makes the viscous effects negligible when calculating the characteristic wave impedance [15]. When neglecting this, the formula for the wave impedance can be expressed as,

$$Z = \sqrt{\frac{L}{C}} \tag{B.1}$$

where L is the inertia and C the compliance [15]. The inertia can be defined as,

$$L = \frac{\rho}{A} \tag{B.2}$$

where A is the cross-section area of the blood vessel cavity and ρ is the blood density [15]. In the blood vessel simulation article by Arts et al. [20] it is stated that the cross-sectional compliance C of the vessel is defined as,

$$C = \frac{A + 0.5A_W}{(k/3 - 1)p_W} \tag{B.3}$$

where k is the wall fiber stiffness, p_W the transmural pressure and A and A_W is the cross-section of the vessel cavity and vessel wall respectively. Input of Equation (B.2) and (B.3) into Equation (B.1) gives the final equation of the impedance,

$$Z = \sqrt{\frac{(\rho/A)}{(A + 0.5A_W)/\Big((k/3 - 1)p_W\Big)}} = \sqrt{\frac{p_W \rho (k/3 - 1)}{A(A + 0.5A_W)}}. \tag{B.4}$$

B.2 Three-wall segment geometry

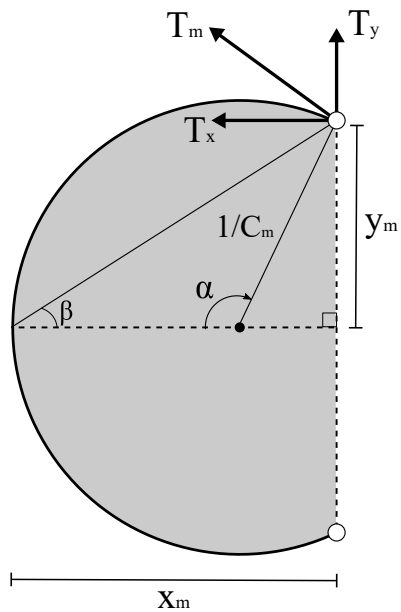

Figure B.1: Three-wall segment geometry. Figure adapted from [21].

Trigonometry and the law of sines give,

$$\frac{\sin\alpha}{\sqrt{x_m^2+y_m^2}} = \frac{\sin\beta}{1/C_m} \tag{B.5}$$

$$\sin\alpha = \frac{\sqrt{x_m^2+y_m^2}\cdot y_m\cdot 2x_m}{\sqrt{x_m^2+y_m^2}\cdot(x_m^2+y_m^2)} \tag{B.6}$$

$$\sin\alpha = \frac{2x_m y_m}{x_m^2+y_m^2}. \tag{B.7}$$

Further trigonometry gives,

$$\cos(\pi-\alpha) = \frac{x_m-(1/C_m)}{1/C_m} \tag{B.8}$$

$$-\cos(\alpha) = \frac{x_m-(x_m^2+y_m^2)/(2x_m)}{(x_m^2+y_m^2)/(2x_m)} \tag{B.9}$$

$$-\cos(\alpha) = \frac{(2x_m^2-x_m^2+y_m^2)/(2x_m)}{(x_m^2+y_m^2)/(2x_m)} \tag{B.10}$$

$$-\cos(\alpha) = \frac{x_m^2-y_m^2}{x_m^2+y_m^2} \tag{B.11}$$

$$\cos(\alpha) = \frac{-x_m^2+y_m^2}{x_m^2+y_m^2}. \tag{B.12}$$

B.3 Linearization and Newtons method

Let $f_1(x_1, x_2)$ and $f_2(x_1, x_2)$ be two differentiable functions in two variables, $f_1(x_1, x_2) : \mathbf{R}^2 \to \mathbf{R}$ and $f_2(x_1, x_2) : \mathbf{R}^2 \to \mathbf{R}$. The linearization of f_1 and f_2 around the point (a_1, a_2) are given by,

$$P_1(x_1, x_2) = f_1(a_1, a_2) + \frac{\partial f_1}{\partial x_1} \cdot (x_1 - a_1) + \frac{\partial f_1}{\partial x_2} \cdot (x_2 - a_2) \quad \text{(B.13)}$$

$$P_2(x_1, x_2) = f_2(a_1, a_2) + \frac{\partial f_2}{\partial x_1} \cdot (x_1 - a_1) + \frac{\partial f_2}{\partial x_2} \cdot (x_2 - a_2). \quad \text{(B.14)}$$

The planes P_1 and P_2 are the tangent planes in (a_1, a_2) to f_1 and f_2 respectively. On matrix form this can be written as,

$$\mathbf{P}(\mathbf{x}) = \mathbf{f}(\mathbf{a}) + \mathbf{J_f}(\mathbf{x})(\mathbf{x} - \mathbf{a}) \quad \text{(B.15)}$$

where $\mathbf{J}_f$ is the jacobian,

$$\mathbf{J_f}(\mathbf{x}) = \begin{bmatrix} \frac{\partial f_1}{\partial x_1} & \frac{\partial f_1}{\partial x_2} \\ \frac{\partial f_2}{\partial x_1} & \frac{\partial f_2}{\partial x_2} \end{bmatrix}. \quad \text{(B.16)}$$

An approximation of $\mathbf{x}$; $\mathbf{x}_k = (x_1,\ x_2)$, can now be improved by using Newtons method. Using the linearization we solve the equation for $\mathbf{P}(\mathbf{x}) = \mathbf{0}$ as such,

$$\mathbf{0} = \mathbf{f}(\mathbf{a}) + \mathbf{J_f}(\mathbf{x})(\mathbf{x} - \mathbf{a}). \quad \text{(B.17)}$$

The solution $\mathbf{x}$ to this equation,

$$\mathbf{x} = \mathbf{a} - (\mathbf{J_f})^{-1}\mathbf{f}(\mathbf{a}) \quad \text{(B.18)}$$

is set to be the new approximation of the variable,

$$\mathbf{x}_{k+1} = \mathbf{x}_k - (\mathbf{J_f})^{-1}\mathbf{f}(\mathbf{x}_k). \quad \text{(B.19)}$$

The theory of Newtons method can now be applied onto the tension components of the walls. Recalling that the tension in the x-direction T_x and the y-direction T_y are functions of the septal midwall volume V and the junction radius Y,

$$T_x = f_1(V, Y) \quad \text{(B.20)}$$

$$T_y = f_2(V, Y). \quad \text{(B.21)}$$

Equation (B.15) can be written as,

$$\underbrace{\begin{bmatrix} T_x^{(k+1)} \\ T_y^{(k+1)} \end{bmatrix}}_{\mathbf{P}(\mathbf{x})} = \underbrace{\begin{bmatrix} T_x^{(k)} \\ T_y^{(k)} \end{bmatrix}}_{\mathbf{f}(\mathbf{a})} + \underbrace{\begin{bmatrix} \frac{dT_x}{dv} & \frac{dT_x}{dy} \\ \frac{dT_y}{dv} & \frac{dT_y}{dy} \end{bmatrix}}_{\mathbf{J_f}(\mathbf{x})} \underbrace{\begin{bmatrix} V^{(k+1)} - V^{(k)} \\ Y^{(k+1)} - Y^{(k)} \end{bmatrix}}_{(\mathbf{x}-\mathbf{a})} \quad \text{(B.22)}$$

where,

$$\frac{dT_x}{dv} = \frac{T_x(V^{(k+1)}, Y^{(k)}) - T_x(V^{(k)}, Y^{(k)})}{dv} \tag{B.23}$$

$$\frac{dT_x}{dy} = \frac{T_x(V^{(k)}, Y^{(k+1)}) - T_x(V^{(k)}, Y^{(k)})}{dy} \tag{B.24}$$

$$\frac{dT_y}{dv} = \frac{T_y(V^{(k+1)}, Y^{(k)}) - T_y(V^{(k)}, Y^{(k)})}{dv} \tag{B.25}$$

$$\frac{dT_y}{dy} = \frac{T_y(V^{(k)}, Y^{(k+1)}) - T_y(V^{(k)}, Y^{(k)})}{dy} \tag{B.26}$$

and dv and dy are calculated as a small fractions of the mean ventricular volume of the heart beat. Rewriting Equation (B.22) and solving for $[T_x^{(k+1)}\ T_y^{(k+1)}] = [0\ 0]$, a new approximation $k+1$ of the septal midwall volume $V^{(k+1)}$ and junction radius $Y^{(k+1)}$ is given by,

$$\begin{bmatrix} V^{(k+1)} \\ Y^{(k+1)} \end{bmatrix} = \begin{bmatrix} V^{(k)} \\ Y^{(k)} \end{bmatrix} - \frac{1}{\det(\mathbf{J}_T)} \begin{bmatrix} \frac{dT_y}{dy} & -\frac{dT_x}{dy} \\ -\frac{dT_y}{dv} & \frac{dT_x}{dv} \end{bmatrix} \begin{bmatrix} T_x^{(k)} \\ T_y^{(k)} \end{bmatrix}. \tag{B.27}$$

Appendix C

Method calculations

C.1 Atrial three-wall segment model

The adapted and included parameter values of the atrial three-wall segment model are determined using geometrical calculations and trial and error. The geometrical calculations were based on a sphere-sphere intersection of the two spherical elements. To minimize the number of changes to the model, the left atrium is simply divided into a left atrial free wall and a septal wall enclosing the left atrium blood volume, as in the modeling of the left ventricle. Thus the material properties of the two walls can be assumed to be the same as the original left wall and fewer parameters need to be estimated.

The four new state variable initial values are calculated as a function of the original model as,

$$y_{m,SAW} = 0.76 \cdot \Big(\frac{4\pi}{3(V_{LA} + 0.5V_{LAW})}\Big)^{1/3} \tag{C.1}$$

$$C_{SAW} = C_{LAW} \tag{C.2}$$

$$L_{si,SAW} = L_{si,LAW} \tag{C.3}$$

and as a function of the new atrial three-wall segment model as,

$$V_{m,SAW} = \frac{V_{SAW}}{2} + 0.08V_{LA}. \tag{C.4}$$

C.2 Radial cylindrical three-wall segment model

The height parameter z is estimated using the initial state of the ventricle of the spherical three-wall segment model. Using the original model initial values of ventricular cavity volumes and septal midwall volume, see Table A.10, and unchanged wall volumes, the left $V_{m,LW}$ and right $V_{m,RW}$ midwall volumes can be calculated from Equation (4.20). The initial junction radius y_m and the midwall x-coordinate

x_m, calculated by Equation (4.22), of each wall then give the initial midwall cross-section area A_{mC}, see Figure C.1, of each wall as,

$$A_{mC} = \left(\frac{x_m^2 + y_m^2}{2x_m}\right)^2 \cos^{-1}\left(\frac{y_m^2 - x_m^2}{x_m^2 + y_m^2}\right) - \frac{y_m(y_m^2 - x_m^2)}{2x_m} \tag{C.5}$$

which follow from geometry. The height z is set to the parameter value giving the same initial left midwall volume $V_{m,LW}$ for the cylindrical model as for the spherical three-wall segment model,

$$z = \frac{V_{m,LW}}{A_{mC,LW}}. \tag{C.6}$$

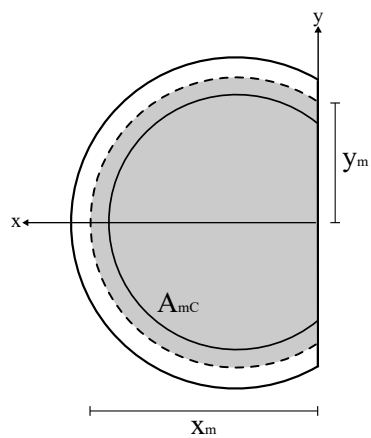

Figure C.1: A cross-section of a spherical segment. The midwall cross-section area A_{mC} (grey area) can be expressed as a function of x_m and the junction radius y_m.

The reference midwall area A_{mRef} of all ventricular walls are determined by performing analysis and calculations on a simulation of the original CircAdapt model. The junction radius y_m is collected at a time point where all three midwall surface areas A_m are close to the parameter values of A_{mRef}. The corresponding x_m of the spherical segments can be determined at the same time point by solving the equation,

$$A_m = \pi(x_m^2 + y_m^2). \tag{C.7}$$

Assuming the same segment dimensions x_m and y_m at reference sarcomere length for the cylindrical model, the new reference midwall area of each wall can be determined geometrically as the arc length at reference sarcomere length multiplied by the fixed cylinder height,

$$A_{mRef} = \frac{x_m^2 + y_m^2}{x_m} \cos^{-1}\left(\frac{y_m^2 - x_m^2}{x_m^2 + y_m^2}\right) \cdot z. \tag{C.8}$$

The initial value of the state variable y_m is unchanged from the original CircAdapt model. The initial value of the septal midwall cross-section area $A_{mC,SW}$ is calculated using Equation (C.5). Using the previously calculated midwall cross-section areas A_{mC} of Equation (C.5), the adapted initial cavity volumes V_{LV} and V_{RV} are calculated as,

$$\begin{cases} V_{LV} &= A_{LV} \cdot z \\ V_{RV} &= A_{RV} \cdot z \end{cases} \tag{C.9}$$

where,

$$\begin{cases} A_{LV} &= A_{mC,LW} - \dfrac{V_{w,LW}}{2z} - \dfrac{V_{w,SW}}{2z} + A_{mC,SW} \\ A_{RV} &= A_{mC,RW} - \dfrac{V_{w,RW}}{2z} - \dfrac{V_{w,SW}}{2z} - A_{mC,SW}. \end{cases} \tag{C.10}$$